Neurophysiological and behavioural investigation of the auditory cortico-collicular pathway



Lee Tai-Ying
李岱穎

Wadham College, University of Oxford

Thesis submitted for the degree of

Doctor of Philosophy

Hilary 2022

For my parents

給爸爸媽媽

Acknowledgements

I have learned and grown a lot during my DPhil, and I feel very lucky and grateful to my family, friends, and colleagues who have supported me at different stages of this journey. This includes but not limited to the people mentioned below.

I would like to thank my supervisors, Prof. Andrew King and Dr. Johannes Dahmen for offering important resources and space for me to develop my skills and to grow as an independent scientist. I would also like to acknowledge the Oxford-Taiwan Graduate Scholarship for the essential financial support for my DPhil study. Additionally, I am grateful to all the members of the lab, particularly Dr. Ben Willmore for his generous support and valuable feedback on my work, as well as Prof. Victoria Bajo and Dr. Fernando Nodal for generously offering intellectual and personal support. I would like to extend my gratitude to all those involved in a major challenge of my DPhil. I would not name them for a reason that they would understand but I remember every single one of them and really appreciate all their support during this difficult time. Thanks also to my SDTA advisors, Dr. Vlad Vyazovskiy and Dr. Dayne Beccano-Kelly, for creating a kind and supportive environment. I am also grateful to Sarah Noujaim, especially when deadlines are a bit tight.

My gratitude also goes to members of my previous research groups and supervisors, especially Prof. Wei-Hsin Sun and Dr. Mehmet Fisek. I really appreciate Wei-Hsin for welcoming this economics undergraduate to the lab and for offering all the support for me to explore and become a neuroscientist. I am grateful to Mehmet and Michael for introducing me to systems neuroscience research. The training and rigour that I have learned have been immensely helpful for my DPhil and beyond. I would also like to thank Dr. Adam Packer for his generous support throughout this journey. I am inspired by his enthusiasm to neuroscience and organised approaches. Special thanks goes to Dr. Tom Bartlett for his valuable feedback on my work and his inspiring passion for statistics research.

My time at Oxford has been enriched by various lovely friends and wonderful communities that I have been lucky enough to be part of. I would like to acknowledge DataKind UK for welcoming me to the friendly and supportive community and offering the opportunities for me to contribute my skills for social good. I am thankful to the members and coaches at Falcon, especially Rajssa Mechelli and

Luca Palmieri for their friendships on and off the water. I am indebted to the instructors at OGC for teaching me how to spread my wings and soar to new heights, particularly ns for always believing in me before I believe in myself. Thanks also goes to OGC members and special mention to Geoff for his limo service. I am grateful to other communities that I was part of that made my DPhil life even more special, including but not limited to Wadham MCR, Cortex Club, ENCODS, Imbizo, I2I, OxAI, OxArt, and various life drawing communities. I must also thank some of my dearest friends, who have made this DPhil journey an extraordinary shared expedition. To Marta Blanco Pozo, together we moved to Oxford (literally) and have had some of the most fun moments and gone through some of the toughest times. To Anna Shpektor for cakes, halloumi, and western dumplings. To tea club Alex Ivanov and Monzy Rahman for their company and heated debates both in and outside the lab. To Leslie Ting-Wei Lin for chats on just about anything and the takeaway rescue. To Bertie Ansell for the walks at different corners of Oxford and for reminding me who I am. To Kharthik Chakravarthy for chats around careers, entrepreneurship, harissa, and the blender.

Heartfelt thanks to Linus Milinski for paddling together through the adventures, and for the care, stability, and balance, especially when the currents get rough.

Finally, I would like to thank my family. To my sister Cheng-Hsuan for being the best partner in crime. To mum and dad for your unconditional support for me to study abroad and pursue a degree that you know little about. I am so grateful for your continuous support and I hope I can make you proud.

Abstract

One of the key objectives in neuroscience is to understand how the brain processes sensory information to generate perception and guide decisions. Sensory processing has been studied extensively, primarily from a hierarchical perspective with a focus on the processing along ascending pathways. However, ascending sensory pathways are accompanied by descending connections at various levels of processing, yet their contributions to sensory processing remain unclear. In this thesis, I studied one of the major descending circuits in the central auditory system, the cortico-collicular pathway, which connects the auditory cortex (AC) to the auditory midbrain (i.e. the inferior colliculus, IC). To understand the role of this pathway during sound-guided behaviour, I used two-photon calcium imaging to measure the activity of neurons in the IC that receive projections from the AC while manipulating the AC inputs during a sound detection task. I found that individual cortico-recipient inferior colliculus (CRIC) neurons exhibited heterogeneous patterns of activity, and that the AC appears to be involved in influencing some of these patterns. Further, I showed that the CRIC trial-by-trial network activity contained behaviourally-relevant information, and that this information was more unreliable when the AC input was removed. Overall, this work offers novel insights into the neural and behavioural function of the auditory cortico-collicular pathway, which contributes to our understanding of the role of descending sensory pathways in perception and behaviour.

Contribution statement

Johannes Dahmen contributed to cranial window implantation, cortical lesions, and imaging experiments. Chris Breen and Johannes Dahmen contributed to histology. The remainder of the thesis is entirely my own work.

Contents

List of Abbreviations **ix**

1 Introduction **1**
- 1.1 Overview of the central auditory system . . . 2
- 1.2 Non-auditory information in the auditory midbrain . . . 4
- 1.3 The auditory cortico-collicular pathway . . . 6
- 1.4 Thesis overview . . . 10

2 Main methods **12**
- 2.1 Animals and Surgeries . . . 13
- 2.2 Sound presentation . . . 16
- 2.3 Behaviour . . . 17
- 2.4 Two-photon calcium imaging . . . 20
- 2.5 Data model . . . 25
- 2.6 Clustering analysis . . . 27
- 2.7 Population decoding . . . 30

3 Sound detection with and without auditory cortical inputs **35**
- 3.1 Learning and performing a sound-guided task with and without AC 36
- 3.2 Development of optogenetics strategies . . . 38

4 Heterogeneous response dynamics of the CRIC neurons **46**
- 4.1 Temporal profiles of average CRIC population response during sound-guided behaviour . . . 47
- 4.2 Heterogeneity of individual CRIC neuronal response patterns during sound-guided behaviour . . . 49

5 Choice-related information in the CRIC network **53**
- 5.1 CRIC network activity contained choice-related information regardless of AC inputs . . . 54
- 5.2 Dynamic contributions of CRIC neurons to the decoding of choice-related information . . . 57

6 Discussion **64**
6.1 Involvement of the AC in sound detection 66
6.2 Manipulation of the CC pathway 67
6.3 Individual neuronal response profiles 68
6.4 Choice-related information in the CRIC network 69
6.5 Neuron contributions to the decoding of choice-related information . 70
6.6 Pre-stimulus activity 71
6.7 Future work 72

Appendices

A Supplementary figures **75**

References **83**

List of Abbreviations

AAV . . . . . Adeno-Associated virus

AC . . . . . Auditory cortex

ANOVA . . . . Analysis of variance

CC . . . . . Cortico-collicular

CNIC . . . . . Central nucleus of the inferior colliculus

CN . . . . . Cochlear nuclei

CRIC . . . . . Cortico-recipient inferior colliculus

dB . . . . . Decibel

DCIC . . . . . Dorsal cortex of the inferior colliculus

IC . . . . . Inferior colliculus

MGB . . . . . Medial geniculate body

NLL . . . . . Nuclei of the lateral lemniscus

PAG . . . . . Periaqueductal gray

PC . . . . . Principal component

PCA . . . . . Principal component analysis

PP . . . . . Peripeduncular nucleus

ROI . . . . . Region of interest

SOC . . . . . Superior olivary complex

SC . . . . . Superior colliculus

SPL . . . . . Sound pressure level

1 Introduction

Contents

1.1 Overview of the central auditory system 2
1.2 Non-auditory information in the auditory midbrain . . 4
1.3 The auditory cortico-collicular pathway 6
1.4 Thesis overview 10

Our perception of the world begins when sensory information reaches our sensory organs and travels through a series of neural signal processing stages from the periphery to the brain. At each stage of sensory processing, the neural representation of the sensory information becomes increasingly abstract and complex. For example, our brain represents visual information from simple segments of the visual world such as the orientation of a line at early stages of processing (Hubel and Wiesel 1962) to objects and faces in higher cortical areas (Haxby et al. 2001). Similarly, the brain represents auditory information from simple elements of the auditory world, including the frequency and amplitude of a sound, to more complex spectrotemporal features that underlie the perception of speech and music (Schnupp et al. 2011). This process of feature extraction has been studied extensively in sensory systems, primarily from a hierarchical perspective. However, ascending sensory pathways are accompanied by descending projections at various stages of processing. Feedback

connections could enable higher-level cognitive and behavioural information from later stages of sensory processing to influence neural activity at earlier stages, making sensory processing a series of dynamic loops instead of being purely unidirectional. Understanding how feedback connections affect sensory processing during behaviour is key to gaining a full picture of how sensory information is processed to generate perception that guides behavioural decisions.

In this thesis, I studied one of the major descending circuits in the auditory system, the cortico-collicular (CC) pathway, which connects the auditory cortex to the auditory midbrain. The goal is to understand how the auditory CC pathway influences animals' behaviour and the responses of the auditory midbrain, which will offer insights into the role of top-down connections in sensory processing and behaviour.

1.1 Overview of the central auditory system

The auditory system transforms pressure waves in our environment into neural signals and representations that allow us to make sense of sound. Following sound processing at the auditory periphery, including the cochlea in the inner ear, acoustic information travels to the cochlear nuclei (CN) in the central auditory system through the auditory nerves (Schnupp et al. 2011). The central auditory system consists of a network of interrelated structures, including the cochlear nuclei, superior olivary complex (SOC), nuclei of the lateral lemniscus (NLL), inferior colliculus (IC), medial geniculate body (MGB), and the auditory cortex (AC) (**Figure 1.1**).

Acoustic information from the CN travels to the auditory midbrain, the IC, via a series of parallel pathways that either project directly to the auditory midbrain or indirectly via the nuclei of the SOC and the NLL (**Figure 1.1**). The IC is subdivided into several regions. The central nucleus of the IC (CNIC), the so-called core or lemniscal region, is the largest and where most ascending inputs terminate (Oliver 2005). The non-lemniscal regions of the IC, including the dorsal and lateral cortices of the IC (collectively referred to as the shell of the IC), receive predominantly ascending inputs but also inputs from the CNIC (Oliver 2005, Chen et al. 2018).

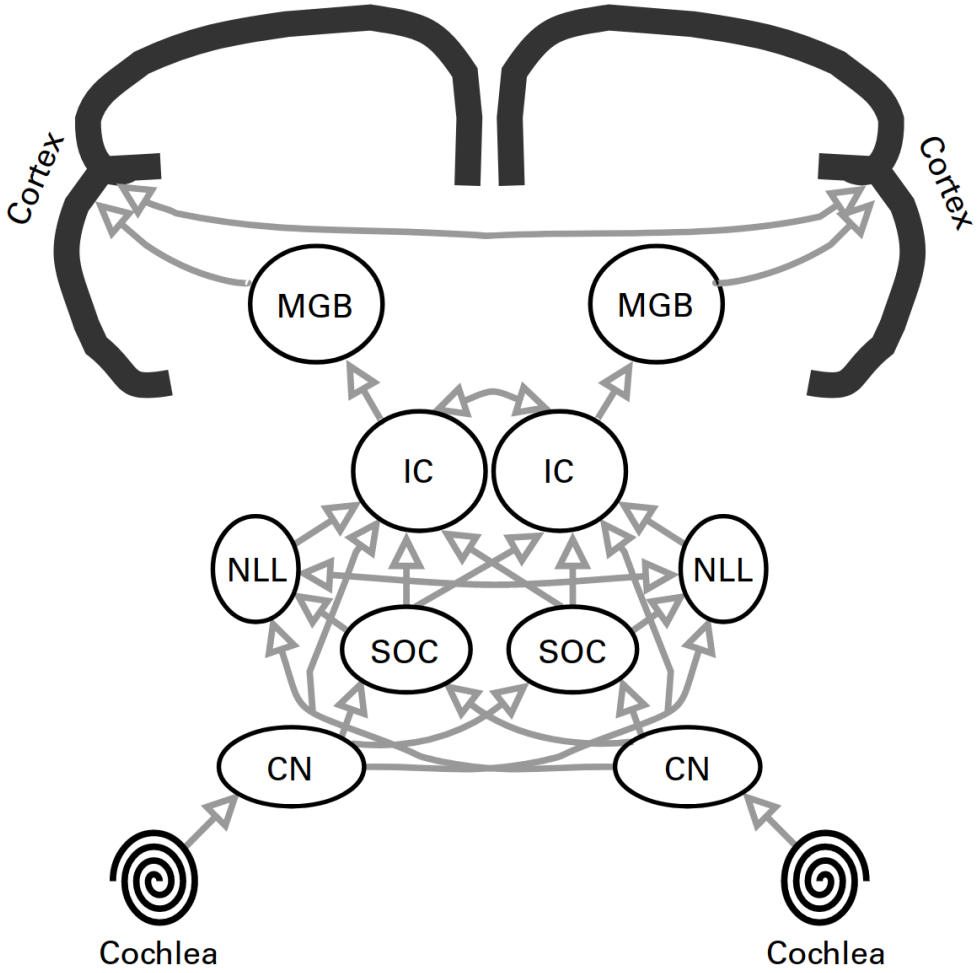

Figure 1.1: Simplified schematic of the feedforward auditory pathways. CN: cochlear nuclei, SOC: superior olivary complex, NLL: nuclei of the lateral lemniscus, IC: inferior colliculus, MGB: medial geniculate body. Figure adapted from Schnupp et al. 2011.

The lemniscal pathway continues from the CNIC to the ventral division of the medial geniculate body (MGBv), which projects mainly to layer 3b and 4 of the primary auditory cortical areas, including the primary auditory cortex and the anterior auditory field (Huang and Winer 2000, Smith et al. 2012). Each of these processing stations of the lemniscal auditory pathway maintains a tonotopic organisation, i.e. neurons in these areas generally have sharp frequency tuning and are generally anatomically-arranged according to their preferred frequency (Stiebler and Ehret 1985, Hackett et al. 2011, Schnupp et al. 2011, Vasquez-Lopez et al. 2017). The non-lemniscal pathway extends from the shell of the IC via the medial and dorsal divisions of the MGB (MGBm and MGBd) (Calford and Aitkin 1983)

to other higher-order areas (Lee and Winer 2008, Vasquez-Lopez et al. 2017).

In addition to these feedforward pathways, there are dense descending projections from the AC to almost every level of the auditory pathway (Winer 2005), including the MGB (Winer and Prieto 2001), IC (Winer et al. 1998), SOC (Mulders and Robertson 2000), and CN (Weedman and Ryugo 1996). The AC also projects to subcortical areas outside of the auditory system, such as the basal ganglia (Reale and Imig 1983) and amygdala (Romanski and LeDoux 1993). The cortico-thalamic projections form recurrent connections between the AC and the MGB (Winer 2005, Llano and Sherman 2008), while the cortico-collicular connections originate most densely from the primary AC and terminate most heavily in the shell of the IC (Herbert et al. 1991, Saldaña et al. 1996, Winer et al. 1998, Bajo and Moore 2005, Bajo et al. 2007, Stebbings et al. 2014). The IC shell also receives descending projections from the auditory thalamus (Adams 1980, Kuwabara and Zook 2000, Senatorov and Hu 2002, Winer et al. 2002, Patel et al. 2017). Since the focus of this thesis is the cortico-collicular pathway, the next sections discuss the anatomy and function of this circuit in more detail.

1.2 Non-auditory information in the auditory midbrain

The IC sits at a central position in the auditory system for integrating top-down inputs from the AC and the converging bottom-up inputs from lower auditory brainstem nuclei (Casseday et al. 2002). In addition to being the centre of convergence for top-down and bottom-up auditory inputs, the IC also receives non-auditory (Olthof et al. 2019, see Gruters and Groh 2012 for review) and neuromodulatory inputs (see Hurley 2018 for review). **Figure 1.2** shows a summary of potential sources of non-auditory inputs to the IC, including inputs from areas that process visual, somatosensory, eye movement signals, and behavioural-context information (Olthof et al. 2019, Gruters and Groh 2012).

Non-auditory information, such as visual and visuomotor signals, are distributed throughout the IC subdivisions, and the responses to these inputs are stronger in

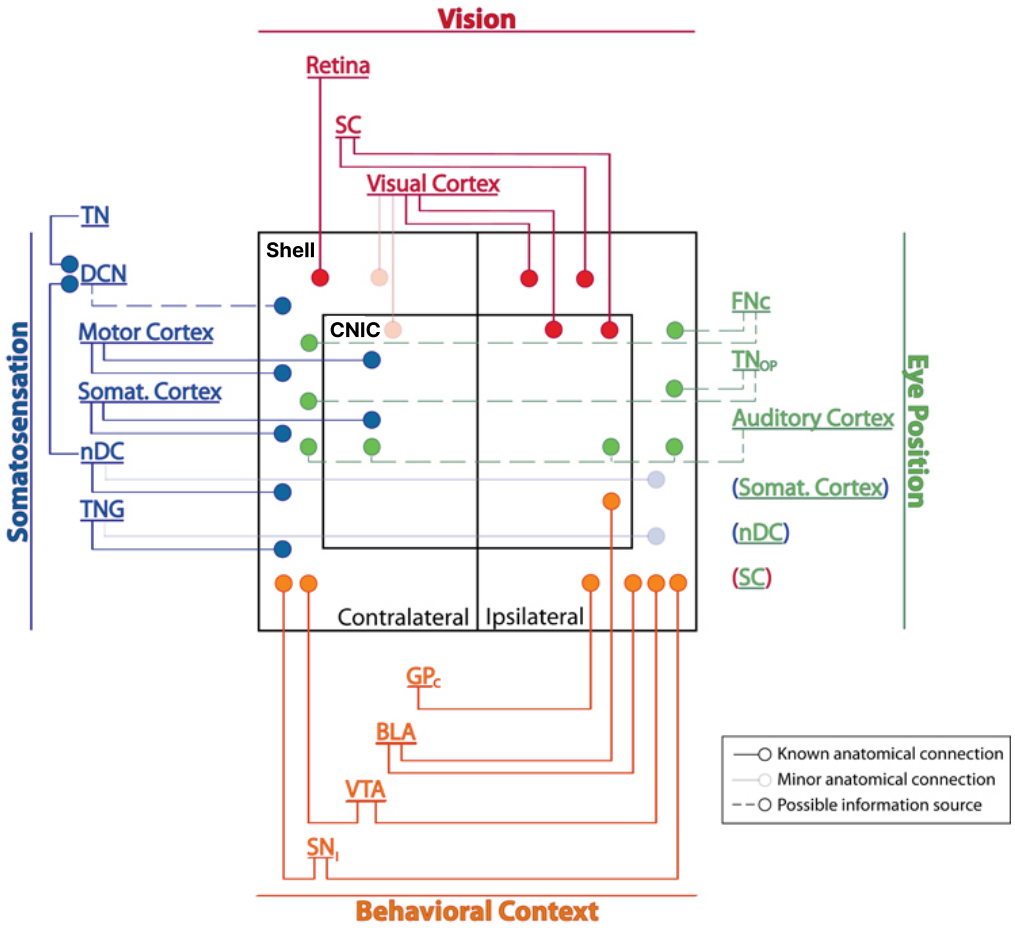

Figure 1.2: Potential sources of non-auditory inputs to the IC. Potential sources of non-auditory inputs from regions that process visual, somatosensory, eye-movement related and behaviourally-relevant information. The somatosensory cortex, superior colliculus (SC), and dorsal column nuclei (nDC) may mediate more than one type of non-auditory input, so they are listed under multiple headings. Their connections to the IC are shown only once, and their potential contribution to another type of inputs is indicated by the colour of the parenthesis. BLA: basal lateral amygdala, CNIC: central nucleus of the IC, DCN: dorsal cochlea nucleus, FNc: fastigial nucleus of the cerebellum, nDC: dorsal column nuclei, SC: superior colliculus, SNi: substantia nigra pars lateralis, TN: trigeminal nerve, TNop: opthalamic tract of the trigeminal nerve, TNG: trigeminal nerve ganglion, VTA: ventral tegmental area. Figure adapted from Gruters and Groh 2012.

the IC shell than in the CNIC (Bulkin and Groh 2012). Somatosensory inputs also modulate the responses of neurons in the IC shell, specifically, the lateral cortex of the IC (Aitkin et al. 1978, Aitkin et al. 1981, Lesicko et al. 2016, Lohse et al. 2021). In addition to multisensory signals, neurons in the IC exhibit locomotion-related activity (Chen and Song 2019, Yang et al. 2020), even in the absence of auditory stimuli and in hearing-impaired mice (Yang et al. 2020). The authors also showed that the tuning selectivity of neurons in the IC shell was decreased during anesthesia compared to the awake state (Chen and Song 2019). Additionally, the IC is sensitive to task engagement, showing generally increased responses in a behavioural task compared to passive listening conditions (Ryan and Miller 1977, Ryan et al. 1984, Metzger et al. 2006). Together, this suggests that the responses of the IC are generally state-dependent. During behaviour, the IC also exhibits increased activity when animals were anticipating an upcoming reward (Metzger et al. 2006).

In addition to receiving non-auditory inputs, the shell of the IC sends projections to diverse targets, including the MGBm, which integrates multisensory and auditory information (Huffman and Henson 1990). The IC shell also projects to the superior colliculus (SC) and the periaqueductal gray (PAG), which are involved in acoustico-motor processing (Huffman and Henson 1990, Xiong et al. 2015).

Together, the diverse circuitry of the IC suggests that this nucleus is well-positioned to not only process auditory information arising from convergent top-down and bottom-up inputs, but also to integrate other sensory, motor, and cognitive information to help shape auditory behaviours. This thesis focuses on investigating how the top-down input from the AC influences the activity of the auditory cortico-recipient IC (CRIC) neurons during behaviour. The goal is to understand whether behaviourally-relevant information is represented in the CRIC neurons, and to what extent this information relies on the AC input.

1.3 The auditory cortico-collicular pathway

The anatomy of the auditory cortico-collicular (CC) pathway has been characterised in several species (Druga et al. 1997, Winer et al. 1998, Winer et al. 2002, Bajo

and Moore 2005, Schofield 2010, Bajo and King 2013, Stebbings et al. 2014). However, the function of these projections during sound-guided behaviour is still poorly understood. This section summarises the anatomy and physiology of the CC pathway, as well as recent studies that aimed to functionally characterise this circuit, including how the CC pathway influences the responses of IC neurons during passive listening conditions and their roles during auditory learning and behaviour.

Anatomy and physiology

The main sources of the auditory CC projections to the IC are pyramidal neurons in layer 5 (L5) and, to a smaller extent, L6 of the ipsilateral primary AC, while a smaller proportion of inputs originate from contralateral AC (Druga et al. 1997, Winer and Prieto 2001, Winer et al. 2002, Bajo and Moore 2005, Schofield 2010, Sekaran et al. 2021). CC neurons in L5 and L6 exhibit distinct physiological properties and receive different sets of cortical and thalamic inputs, and are thus thought to have different functional roles in the CC pathway (**Figure 1.3**, Slater et al. 2013, Slater et al. 2019, Yudintsev et al. 2021). At the synaptic level, results from two studies have together indicated that the top-down CC input and the bottom-up sound-driven responses could arrive at the IC with potential temporal overlap (Williamson and Polley 2019, Oberle et al. 2022). By stimulating axons from both ascending and descending pathways to the IC shell *in vitro*, Oberle et al. 2022 further showed that these signals could be integrated non-linearly in the IC shell. This provides an important synaptic basis for understanding how CC projections might contribute to the responses of neurons in the IC shell during auditory learning and behaviour.

Passive listening

Early studies showed that focal electrical stimulation or inactivation of the AC could induce changes in the sensitivity of IC neurons to sound frequency (Yan and Suga 1998, Zhang and Suga 2000, Ma and Suga 2001b, Yan et al. 2005, Suga et al. 2002), amplitude (Yan and Ehret 2002), duration (Ma and Suga 2001a), and location (Nakamoto et al. 2008). More recently, Barnstedt et al. 2015 recorded the activity of CC axons and neurons in the dorsal IC to map their response properties in

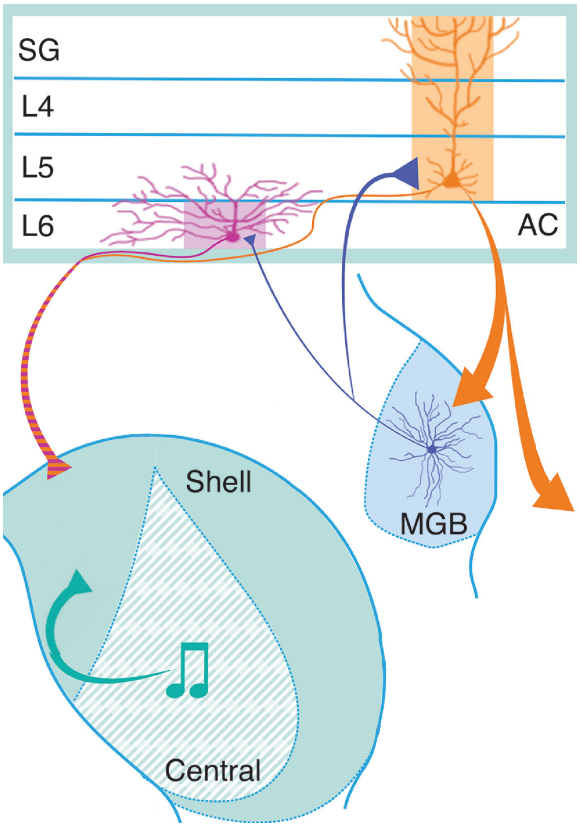

Figure 1.3: Recent findings of the anatomy and physiology of the CC pathway. CC neurons in L5 of the AC are pyramidal neurons and receive input from L5 and all other cortical layers superficial to it, while CC neurons in L6 receive inputs mostly from the local layer (Slater et al. 2013, Slater et al. 2019). L5 CC neurons receive direct excitatory thalamic input, while a smaller proportion of L6 CC neurons do (Slater et al. 2019). Feedforward sound-driven responses and feedback CC activity reach the IC with potential temporal overlap, and their signals can be integrated non-linearly in the shell of the IC in slice recordings (Oberle et al. 2022). SG: Supragranular layers. Figure adapted from Lesicko and Geffen 2022.

anaesthetised mice. They found that acoustically responsive CC boutons were sparse and exhibited unreliable responses, while the response properties of the neurons in the dorsal cortex of the IC (DCIC) were similar to those of dorsal CNIC (Barnstedt et al. 2015). Another recent study utilised optogenetics to selectively manipulate auditory cortical neurons projecting to the IC in awake and anaesthetised mice (Blackwell et al. 2019). They found that activation of these neurons moderately increased spontaneous activity and decreased stimulus selectivity of IC neurons, while inactivation had no effect (Blackwell et al. 2019). Optogenetic inactivation of auditory cortical neurons also had no effect on contrast gain control exhibited in

the CNIC in either anesthetized or awake mice (Lohse et al. 2020). While these results support the hypothesis that the influence of the CC connections may only become apparent when animals are engaged in tasks that involve active listening and behaviour (Bajo et al. 2010, Price and Bidelman 2021, Souffi et al. 2021, Lesicko and Geffen 2022), another recent study has shown that optogenetic inactivation of the CC pathway resulted in a decrease in prediction error signals in the IC (Lesicko et al. 2022), indicating that the CC projections could potentially be involved in shaping the responses of the IC during processes such as predictive coding.

Plasticity, learning, and behaviour

The auditory CC pathway has been implicated in auditory plasticity, learning, and other aspects of behaviour (Bajo et al. 2010, Xiong et al. 2015, Asokan et al. 2018). Bajo et al. 2010 showed that ablation of the CC pathway did not affect animals' ability to localise sound, but did impair their ability to adapt to unilateral hearing loss in order to re-learn to localise sound accurately. This indicates that the CC pathway is involved in re-calibrating the brain's representation of auditory space. Another study found that the responses of CC axon terminals in the IC were strongly depressed following peripheral nerve damage. Nevertheless, enhanced responses were found by the following day and lasted for several weeks, even though the auditory nerve input had been persistently reduced (Asokan et al. 2018). This suggests that the CC pathway is recruited following auditory peripheral damage, and the persistent elevated responses could be associated with tinnitus or acting as a mechanism for the auditory system to maintain auditory perception after peripheral nerve damage (Asokan et al. 2018, Lesicko and Geffen 2022). The CC pathway has also been shown to be involved in driving sound-induced defence behaviour (Xiong et al. 2015). Optogenetic activation of auditory L5 neurons and their axons in the IC shell both elicited flight behaviour, while optogenetic inactivation reduced the noise-induced flight behaviour (Xiong et al. 2015). Additionally, the authors showed that the CC input to the shell of the IC drove these defense responses through the IC shell's projections to the dorsal–lateral part of the periaqueductal

gray (dPAG) (Xiong et al. 2015), which is involved in acoustico-motor processing. This suggests that the CC pathway is involved in sound-induced defense behaviour through an AC-IC-dPAG circuit.

Summary and future directions

As outlined above, the auditory CC pathway has been implicated in various aspects of auditory processing, plasticity, and behaviour. However, most studies have focused only on the influence of the AC on the activity of neurons in the CNIC, even though AC input terminates most heavily in the shell of the IC. It is also unclear from most previous studies whether the IC neurons from which recordings were made received AC inputs or not. Additionally, research studying the effects of activating or inactivating the AC on the responses of IC neurons was typically performed in either anaesthetised or passive listening conditions, while the CC pathway may play a different role during behaviour (Ryan and Miller 1977, Ryan et al. 1984, Souffi et al. 2021). Studies conducted in behaving animals have investigated how manipulating the AC resulted in changes in the animals' behaviour, leaving the neural correlates of the behavioural change largely unexplored. Together, this suggests that, to fully understand the behavioural and physiological function of this major descending pathway, it is essential for future research to record the activity of neurons in the IC while manipulating the AC input during behaviour. In this thesis, I utilised recent advances in viral tools and imaging techniques to record from neurons in the IC that receive direct AC input, while manipulating the AC during sound-guided behaviour. The goal of this work is to gain insights into the responses of cortico-recipient IC (CRIC) neurons during the sound-guided behaviour, and how they change when the AC input was silenced.

1.4 Thesis overview

This thesis aims to understand how descending connections from the AC influence the responses of IC neurons during sound-guided behaviour. By imaging cortico-recipient IC (CRIC) neurons (i.e. neurons that receive direct input from the AC) specifically,

the effect of the AC input on the IC could be more precisely dissected. In this work, I automated a behaviour training paradigm for efficiency and reproducibility, and recorded the activity of the CRIC neurons while the mice learned and performed a sound detection task. We set out to study the effects of both chronic and acute inactivation of the cortico-collicular input. However, despite exploring, testing and documenting a number of different approaches, acute suppression of the CC axons with optogenetics could not be implemented satisfactorily, we therefore had to rely on the chronic removal of the AC input. In addition, I developed a data management system to store and process data, and performed analysis of the neural and behavioural data to gain insights into the influence of the AC on the responses of CRIC neurons and the ability of mice to learn and perform a sound-guided task. Overall, the hope is that this thesis will offer insights into the neural and behavioural function of the auditory cortico-collicular pathway. This will in turn improve our understanding of the role of descending projections in the brain in sensory processing and behaviour, an important element of the neural computation for us to perceive the world and guide our decisions.

2
Main methods

Contents

2.1 Animals and Surgeries 13
2.1.1 Animals 13
2.1.2 Intracranial injection 13
2.1.3 Cranial window implantation 14
2.1.4 Cortical lesions 15
2.1.5 Histology 15
2.2 Sound presentation 16
2.2.1 Tone presentation with optogenetic stimulation 16
2.2.2 Data analysis 16
2.3 Behaviour 17
2.3.1 Paradigm 17
2.3.2 Performance analysis 19
2.3.3 Quality control 20
2.4 Two-photon calcium imaging 20
2.4.1 Acquisition 20
2.4.2 Image processing 21
2.4.3 Quality control 24
2.5 Data model 25
2.5.1 Relational databases 25
2.5.2 ETL Pipelines 27
2.6 Clustering analysis 27
2.7 Population decoding 30

All experiments were performed in accordance with the Animals (Scientific Procedures) Act 1986 and under a Project Licence regulated by the UK Home Office,

following approval by the local ethical review committee at the University of Oxford.

Code availability

The code for analysis will be available at `https://github.com/leetaiying`.

2.1 Animals and Surgeries

2.1.1 Animals

42 Ai95(RCL-GCaMP6f)-D (Jackson Laboratories; stock number 024105; Ai95D for short) transgenic mice aged between 9-15 weeks during imaging experiments were used. After Cre exposure, these mice express a calcium indicator, GCaMP6f (Chen et al. 2013), which allows indirect readout of neuronal activity using two-photon calcium imaging.

For the optogenetics experiments, the following transgenic mouse lines were used: 7 Rbp4-Cre KL100 mice (Rbp4-Cre for short) for targeting Rbp4-positive neurons, which are mainly in layer 5 of the cortex; 3 CaMKIIα-Cre-3487 mice for targeting CaMKIIα-positive neurons (excitatory neurons); and 3 mice from a GCaMP6f reporter line, produced by mating the Ai95D line (Jackson Laboratories; stock number 024105) with the CaMKIIα-Cre T29–1 line (Jackson Laboratories; stock number: 005359), referred to as CaMKIIα-Cre-GCaMP6f mice in Chapter 3.2.

2.1.2 Intracranial injection

Mice were anaesthetised with 1.5-2% isoflurane during all surgical procedures (5% for induction). To specifically express GCaMP in IC neurons that receive auditory cortical inputs, mouse was fixed on a stereotaxic frame and 150-200 nl (in total) of AAV1-hSyn-Cre (Penn Vector Core) were injected unilaterally in three sites in the AC of Ai95D mice at depths of 450-550 µm below the brain surface. AAV1-hSyn-Cre has been shown to have anterograde transsynaptic properties (Zingg et al. 2017), allowing the expression of Cre in cortico-recipient IC neurons. This enabled us to drive the expression of GCaMP in those neurons in transgenic mice expressing Cre-dependent GCaMP. Note that AAV1-hSyn-Cre can also retrogradely spread

to presynaptic neurons with low efficiency, however, to the best of our knowledge, no study has shown that the IC projects to the AC. Mice were checked daily for their wound, weight, behaviour, and general appearance for a few days following the surgery to monitor the recovery. The post-surgery check was also carried out after all the other surgical procedures mentioned below.

To develop viral strategies for optogenetics experiments, 7 combinations of viruses and mouse lines were attempted (**Table 3.1**). To express opsins in auditory cortico-collicular axons, 26 Ai95D mice were used to combine AAV1-hSyn-Cre with 3 different opsins (AAV8-CAG-FLEX-Jaws-tdTomato, AAV5-hSyn-eNpHR3.0-mCherry, and AAV1-CAG-Flex-Jaws-tdTomato). Additionally, 7 Rbp4-Cre mice were used to express opsins in cortical layer 5 neurons, and 6 mice expressing CaMKIIα were used to express opsins in excitatory neurons (3 CaMKIIα-Cre-GCaMP6f and 3 CaMKIIα-Cre-3487). The injections in the AC were 200 nl in total volume and spread across three sites at two depths between 550 - 450 µm below the surface, while the injections in the IC were 150 nl in total volume and spread across 4 - 6 sites at two depths between 250-150 µm below the surface. When two viruses were injected in the AC, they were mixed 1:1 in volume. All injections were made unilaterally, except that two of the Ai95D mice injected with AAV1-flex-jaws were injected bilaterally in the AC.

2.1.3 Cranial window implantation

3-8 weeks after intracranial injection, mice were anaesthetised using the same procedure described above, and a craniotomy (3 mm in diameter) was made over the IC in the right hemisphere (close to lambda). A glass window of the same size was glued to a 1 mm steel cylinder and implanted over the IC to offer optical access for monitoring neural activity longitudinally. To allow head fixation of the mouse during two-photon calcium imaging, a custom-made head plate was fixed on the mouse's skull with dental acrylic (Superbond CB).

Roughly 85% of the unlesioned mice that had undergone surgeries were used for imaging experiments reported in this thesis, and it dropped to about 60% for

lesioned mice. The most common reason for not being able to perform further experiments on a mouse is excessive blood loss during the surgery, due to either damage to the transverse sinus close by or as a result of the lesioning procedure. Imaging experiments were also not performed when the cranial window was occluded by blood accumulated below the window for a few days after the surgery.

2.1.4 Cortical lesions

In 8 mice, bilateral lesions of the auditory cortex were carried out before cranial window implantation during the same surgery. Craniotomies of approximately 3 mm in diameter were made over the auditory cortices in both hemispheres. The underlying cortical tissue was either removed by aspiration (Hong et al. 2018) using a sterile, blunted 19 G syringe needle connected to a vacuum (3 mice), or by thermocoagulating (Ceballo et al. 2019) with a cauterizer (Small Vessel Cauterizer Kit, FST 18000-00, Germany) held close to the cortical surface for several seconds (5 mice).

To visualise the number of IC-projecting cortical neurons left after cortical lesions, at the end of experiments, a subset of mice were injected with 150 nl of retrograde viruses (rAAV2-retro-tdTomato, UNC Vector Core) into the IC across three sites at depths of 100-400 µm below the brain surface after imaging experiments were completed and 2-3 weeks before perfusion.

2.1.5 Histology

After imaging experiments were completed, mice were perfused transcardially and fixed with phosphate buffered saline and 4% paraformaldehyde. Each brain was sectioned coronally (100 µm thick) with a vibratome (Leica). Brain sections were viewed and images were taken using a confocal laser scanning microscope (Olympus FV1000) with a 10x or 20x objective.

The extent of lesions was estimated by a colleague blind to the results, using histological images referencing a mouse brain atlas (Paxinos and Franklin, 2001). The images were inspected and given a score of "(near-)complete" or "partial" for each mouse. There were 4 mice scored with "(near-)complete" and 4 mice

scored with "partial". In the mice where cortical lesions were performed with aspiration, the lesions tended to extend into subcortical tissues such as the striatum. Further analysis is currently being done to examine how the extent of lesions correlate with the results.

2.2 Sound presentation

2.2.1 Tone presentation with optogenetic stimulation

To assess how optogenetically silencing AC axons influences the responses of neurons in the IC, two-photon calcium imaging was performed while tones were presented to the mice injected with opsins few days after cranial window implantation. A total of 16 pure tones were presented at 60 dB SPL (100 ms duration, 1.5 seconds inter-trial interval) and each tone was presented 30 times in total. The frequency of the tones were varied randomly from 2 kHz to 64 kHz in 1/3 octave steps. Tones were presented via a thin silicone tube coupled to an electrostatic loudspeaker (EC1, Tucker-Davis Technologies, FL, USA), placed near the entrance of the mouse's left ear canal. The drivers was calibrated using a G.R.A.S. 40DP (G.R.A.S., Denmark) microphone to ensure a flat (±3 dB) response at all presented frequencies. In 50% of the trials, the tones were paired with optogenetic laser stimulation beginning 25 ms prior to the tone onset and lasted for 150 ms. Laser on and laser off trials were randomly interleaved. The stimuli were generated with an RZ6 processor (Tucker-Davis Technologies) and controlled through custom-written MATLAB (MathWorks, MA, USA) code.

2.2.2 Data analysis

The following analysis steps were performed to examine the effect of silencing AC axons on the responses of IC neurons. For each neuron, the Shapiro-Wilk test was used to test if the responses were normally distributed. Based on the results of the Shapiro-Wilk test, a one-way ANOVA (for normally distributed responses) or Kruskal-Wallis H-test (for non-normally distributed responses) was performed across all the combinations of sound frequencies and laser conditions (on vs off) for each

neuron. Only neurons with $p < 0.05$ (i.e., responsive to at least one of the sound and laser combinations) were included in the subsequent analysis. The response in each trial was defined as the average of ~300 ms of neuronal activity starting ~250 ms after the tone offset. The omission of the first 250 ms after tone offset was to ensure responses were not included when the laser stimulation was present. To compute the best frequency of each neuron, the responses to the same sound frequencies were summed together regardless of the laser conditions, and the tone that elicited the maximum response was defined as the best frequency. To assess the effect of inhibiting AC axons on the activity of IC neurons, a one-sided paired t-test (for normally distributed responses) or Wilcoxon signed-rank test (for non-normally distributed responses) was done across neurons using the responses to their respective best frequencies. The summary figures were produced by aligning each neuron's responses with its best frequency at the centre, separated by laser conditions.

2.3 Behaviour

To understand the role of CRIC neurons in sound processing and sound-guided behaviour, mice were trained to perform a sound detection task. Two-photon calcium imaging was performed while the mice learned and performed the task, allowing us to characterise the neural representations during learning and behaviour.

2.3.1 Paradigm

Around 2-3 days before the start of the training, mice were habituated daily to get used to handling and the experimental setup. Mice also received ~1 ml of water per day, bringing their body weight down to ~85% of the weight before water restriction.

The sound detection task required the mouse to report a 0.5 ms broadband click stimulus by licking within a response window to trigger a water reward (2 µl) from a lick port in front of the mouse. Stimulus trials and catch trials (i.e. trials where no stimulus was presented) were randomly interleaved with an inter-trial interval that was drawn from a normal distribution with a mean of 8 s and a standard deviation of 2 s, with a minimum of 3 s. Catch trials were introduced to estimate the baseline

response rate of each mouse in a given session. In a stimulus trial, if the mouse successfully reported the detection of the sound within the response window, the trial was scored "hit", while failure to respond was scored "miss". In a catch trial, if the mouse licked during the respond window, it was scored "false alarm", while if the mouse withheld licking during the response window, it was scored "correct rejection".

During the initial passive training phase, the click stimulus was presented at 80 dB sound pressure level (SPL) and a reward was automatically delivered immediately following a stimulus. This was to train the mouse to associate the sound with the water reward. After the mouse successfully responded within the 2-second response window for 3 consecutive trials, it would transition into the active training phase for the rest of the session, where the mouse had to respond within the respond window to trigger the water reward in stimulus trials. A reward was delivered immediately following a correct response. During this early stage of training, mice sometimes failed to maintain a consistent behavioural performance. To remind the mouse of the task, after 3 consecutive miss trials, a reward was automatically delivered in the next stimulus trial. Mice were trained daily to perform the task and the behaviour training pipeline was automated to ensure reproducibility[1].

Once a mouse achieved a d' > 1.5 for a given session for at least 2 days (see **Performance analysis** for the definition of d'), quieter stimuli (41-71 dB SPL, with 3 dB spacing) were introduced to increase the uncertainty of the task[2]. The range of sound levels introduced depended on the behavioural performance in each session.

For the optogenetics experiments, during the training phase, the optogenetic laser stimulation was present in every trial to assess whether inhibiting cortico-collicular axons influences learning. The laser stimulation began 25 ms prior to the click onset and lasted for 65 ms. In the subsequent testing phase where multiple

[1]Experiments conducted by colleagues started with the active training phase directly and did not use the automated behaviour training pipeline. If the mouse did not respond to the stimulus, rewards were delivered manually at times based on colleagues' judgements.

[2]For the experiments conducted by colleagues, the response window in some sessions was reduced to either 0.5 or 0.75 seconds to discourage excessive licking.

sound levels were presented, the clicks were paired with the laser stimulation in all the trials in early sessions and in around 50% of the trials in later sessions.

The behavioural experiments were run using custom MATLAB (MathWorks) scripts interfacing with a National Instruments board (NI USB-6501) for reward delivery and lick registration. The stimuli were presented using Psychtoolbox through a free-field speaker (Vifa, Avisoft Bioacoustics, Germany), positioned ~15 cm from the snout of the mouse.

2.3.2 Performance analysis

Behavioural performance was assessed by calculating the sensitivity index, d' (Brophy 1986), which quantified the difference in the probability of response (i.e., licking) between stimulus and catch trials. Specifically, this involved calculating the difference between the z-transform of the hit and false alarm rates:

$$\mathbf{d'} = \mathbf{z}(\text{hit rate}) - \mathbf{z}(\text{false alarm rate}) \tag{2.1}$$

When mice were well-trained, they could sometimes achieve 100% hit rate or 0% false alarm rate in a session. Since the z-transform of 1 and 0 approaches positive and negative infinity, respectively, the hit and false alarm rates were adjusted (Hautus 1995; Stanislaw and Todorov 1999) as described in Equations 2.2 and 2.3, where **N** was the number of trials for the respective trial types within a given session.

$$\textbf{Hit rate} = \frac{\mathbf{N}_{\text{hit}} + 0.5}{\mathbf{N}_{\text{hit}} + \mathbf{N}_{\text{miss}} + 1} \tag{2.2}$$

$$\textbf{False alarm rate} = \frac{\mathbf{N}_{\text{false alarm}} + 0.5}{\mathbf{N}_{\text{false alarm}} + \mathbf{N}_{\text{correct rejection}} + 1} \tag{2.3}$$

A mouse was considered to have "learned" when d' was greater than 1.5 for a given session. The detection threshold was defined as the lowest sound level at which the mouse achieved the performance that was defined as learned in each session.

2.3.3 Quality control

Sessions were split into blocks so that the field of views could be checked and adjusted for z drift if necessary. The number of blocks in each session varied across sessions, and was dependent on the mouse's behaviour. Typically 3-6 blocks were carried out within a session. Each block of imaging lasted either ~8 or ~16 minutes. Within a session, the mouse's performance sometimes dropped sharply in the last block, likely due to satiation of the water reward. Including these blocks when conducting the behavioural performance analysis (see **Performance analysis** in the previous section) might underestimate the mouse's behavioural performance. Therefore, the last block of a session was excluded from analysis if the mouse achieved a d' > 1.5 for the 80 dB SPL stimulus in all the blocks other than the last block.

Additionally, hit trials were excluded from analysis if any licks occurred between -0.5 to +0.12 seconds relative to stimulus onset (Kwon et al. 2016), as these licks were likely not driven by the stimulus.

2.4 Two-photon calcium imaging

2.4.1 Acquisition

Mice were habituated to head-fixation under the two-photon microscope 2-3 days prior to imaging experiments. Each imaging session lasted around 1-2 hours in duration. Tens to hundreds of neurons were recorded simultaneously close to the dorsal surface of the IC at a depth of 50-150 µm.

Two-photon calcium imaging was performed using a commercial two-photon microscope (B-Scope, Thorlabs) with a 16x 0.8 numerical aperture (NA) water immersion objective (Nikon). GCaMP6f was excited at 930 nm (10-50 mW at specimen) with a SpectraPhysics Mai-Tai laser. Acquisition was controlled using ScanImage (Pologruto et al. 2003) at approximately 27 Hz depending on the size of the imaging field of view. The imaging field of view is either 500 x 500 µm (11 and 30 sessions from unlesioend and lesioned mice, respectively) or 666 x 666

µm (29 and 13 sessions from unlesioend and lesioned mice, respectively) with a resolution of 512 x 512 pixels.

For the optogenetics experiments, a 640 nm laser pulse (150 ms duration) (iBEAM-SMART-640-S, Topica) of 60 mW was delivered via a 400 um optical fibre positioned over the cranial window. Two LEDs (625 nm) (M625F2, Thorlabs) were coupled to optic fibres and positioned directly in front of the mouse's eyes to mask the light from the laser stimulation.

2.4.2 Image processing

Image processing, including registration, segmentation, and signal extraction were performed using the Python version of suite2p (Pachitariu et al. 2017 bioRxiv), a pipeline for processing two-photon calcium imaging data.

Registration

Image registration is the process of aligning images to the same coordinate system. It is an essential step for processing brain imaging data since brain motion during recordings is unavoidable, and the resulting displacement of images could cause apparent changes in the activity of neurons while in fact reflecting motion artefacts.

Behavioural tasks in rodents often involve motor outputs as read-outs of decisions, including licking, lever pressing, nose poking, and running. Such motor behaviours could induce excessive brain movement during imaging and cause apparent "task-evoked" responses. Displacement of images resulting from this are often assumed to be rigid (i.e., the whole image shifts in the same way) and the X/Y displacement can be detected and corrected by image registration algorithms (Stringer and Pachitariu 2019). Another type of brain motion that could confound the recorded activity of neurons is the deformation of the brain induced by factors such as haemodynamics and temperature change (Stringer and Pachitariu 2019). It usually happens at a slower timescale of tens of minutes and can lead to changes in recorded baseline fluorescence over the course of an imaging session. A common way of addressing this is by subtracting a running baseline. At the extreme case, such

deformation of the brain could result in different groups of neurons being recorded at the beginning and the end of a session.

The registration algorithms for two-photon imaging mostly only address the brain motion in the X/Y plane, since Z-motion usually leads to smaller changes in signals due to the more elongated point spread function along the Z-axis compared to the X and Y axes (Helmchen and Denk 2005; Chaigneau et al. 2011). However, Z-motion could cause neurons to move in and out of the imaging plane and confound the recorded neural activity. While online correction for Z-motion during imaging is possible, it is not widely employed. Thus, quality control is an essential step in addition to the computational processing by image registration algorithms (see 2.4.3).

Two-photon imaging data in this thesis were registered with suite2p. The algorithm extends phase correlation to detect the displacement between each frame and a target image, where the target image is the average of randomly sampled frames that have been iteratively aligned. After the displacements were computed, the frames were shifted in the Fourier domain, which allows sub-pixel shifts (down to 1/10 of a pixel) of the images. Both rigid and non-rigid (i.e., parts of the images shift in different ways) registration were performed. The non-rigid registration divided the image into segments and computed the shifts for each segment separately. The registered images were then ready for segmentation.

Segmentation

Image segmentation is the process of partitioning an image into multiple segments that are often more meaningful to analyse. In the case of two-photon imaging, we need to identify the pixels representing neurons or neuronal processes to allow subsequent analyses.

In recent cell segmentation pipelines, activity-based criteria are often used instead of morphology-based criteria. This is because, while sparsely active cells are not distinctly visible in mean registered images, they are detectable using functional methods such as the activity correlations between pixels. Additionally, if cells are detectable in mean images but not with activity-based methods, their fluorescence

only reflects the baseline values. These cells often have unhealthy calcium dynamics or have extremely sparse activity that can be discarded for further analysis.

The algorithm in suite2p uses activity-based methods to detect regions of interest (ROIs), i.e. neurons or neuronal processes. It first reduces the dimensionality of the registered images to find the top spatial principal components. This step allows the data to be denoised as well as reducing the space and time required to store and process the data. To detect ROIs in these spatial components, an iterative algorithm is performed to smooth the components, detect peaks in the correlation map (i.e., weighted "multi-dimensional correlation" for each pixel with the surrounding pixels) for these components, and then extend the ROIs spatially around these peaks. The output of this stage was a set of spatial ROIs ready for signal extraction.

Signal extraction

The fluorescence time-series for individual ROIs could be obtained by averaging over all the pixels belonging to the same ROI at each time point. However, these signals often contain out-of-focus fluorescence ("neuropil"), which reflects the averaged activity of passing neuronal processes and has been shown to be stimulus-dependent and behaviour-related (Chen et al. 2013; Peron et al. 2015; Lee et al. 2017). Thus, it is important to separate the activity of neuropil from somatic activity when drawing scientific conclusions (Harris et al. 2016; Lee et al. 2017).

In suite2p, the generative model of the recorded fluorescence signals $\mathbf{F}_i$ for a given ROI i is the sum of the somatic signals from a spike train $\mathbf{s}_i$ convolved with a calcium response kernel $\mathbf{k}_i$, the neuropil signals $\mathbf{N}_i$ scaled with a coefficient c_i, and Gaussian noise:

$$\mathbf{F}_i(t) = [\mathbf{s}_i * \mathbf{k}_i(t)] + c_i\mathbf{N}_i(t) + noise \tag{2.4}$$

The standard practice for estimating neuropil signals $\mathbf{N}_i$ is to average the pixel values surrounding each ROI (Chen et al. 2013; Pachitariu et al. 2017). The values for each ROI are then scaled with $c = 0.7$ for all neurons before subtracting from $\mathbf{F}_i$ (Chen et al. 2013; Peron et al. 2015).

To obtain $\mathbf{F}_i$ for each ROI, the standard practice outlined above was followed. The $\mathbf{N}_i$ was computed by the suite2p algorithm and the scaling and subtraction of $\mathbf{N}_i$ were done after manual curation of the ROIs (see 2.4.3).

2.4.3 Quality control

Sessions were excluded from analysis if there was excessive displacement in the Z-axis observed affecting most of the ROIs in the field of view, since this could confound the recorded neural activity as described in **Registration** in 2.4.2. ROIs in each imaging session were manually selected after inspecting the registration metrics and lick-triggered time series as described below.

Registration metrics

To examine the quality of the registration, the spatial principal components (PCs) of the registered images (computed with suite2p) were inspected. By comparing the average of the top and bottom 500 frames of each PC, displacement in the Z-axis could be detected. Any ROI with excessive displacement in the Z-axis observed was discarded from further analysis.

Lick-triggered time series

To inspect the extent of the displacement of the imaging plane caused by motor outputs of the task (i.e., licking), lick-triggered movies of the imaging field of views were created for each session. This is based on the assumption that licks triggered stereotypical displacement of the imaging plane, which would be apparent when images were averaged across lick events. Specifically, raw images (without registration) of each field of view were averaged 2 seconds before and after each lick event. Depending on the length of the session, 3-6 movies were created for each session. The lick-triggered movies were then examined in combination with raw images to determine if there was excessive displacement in the Z-axis. ROIs were excluded from subsequent analysis if any excessive Z-motion was identified.

2.5 Data model

Scientific data have increased in both scale and complexity in recent years. Thus, data organisation becomes increasingly important to ensure the integrity of the data and the efficiency to perform subsequent analyses. One way of achieving this is to design a data model, which is a conceptual framework that defines the structure of the data, the relationships between them, and the operations to be performed on them. Here, I developed a system to store and process data, which includes relational databases, "extract, transform, load" (ETL) pipelines, and automatic analyses, utilising a refined relational data model, datajoint (Yatsenko et al. 2018).

2.5.1 Relational databases

The use of relational databases allows us to define the structure of the stored data, to flexibly access subsets of data with querying languages, and to maintain data integrity (Codd 1970). Maintaining data integrity is an essential part of data management, which includes ensuring that there are no duplicate data and that dependencies between data are correctly maintained (e.g. if data B is dependent on data A, then data B should not exist if data A is missing). This was achieved by utilising datajoint (Yatsenko et al. 2018), a scientific data model with a particular focus on data integrity.

Data in this thesis, including text data with trial information as well as the preprocessed calcium imaging data (see 2.4.2) were stored in relational databases hosted on Docker, a tool to build and deploy applications with operating-system-level virtualisation. Data were stored in the forms of relations (i.e. tables) in relational databases, and related to each other by their shared attributes (i.e. columns) (Codd 1970). Tables were assigned to different categories depending how the data originated (Yatsenko et al. 2018), including the following:

- Manual: Tables that require manual entry.

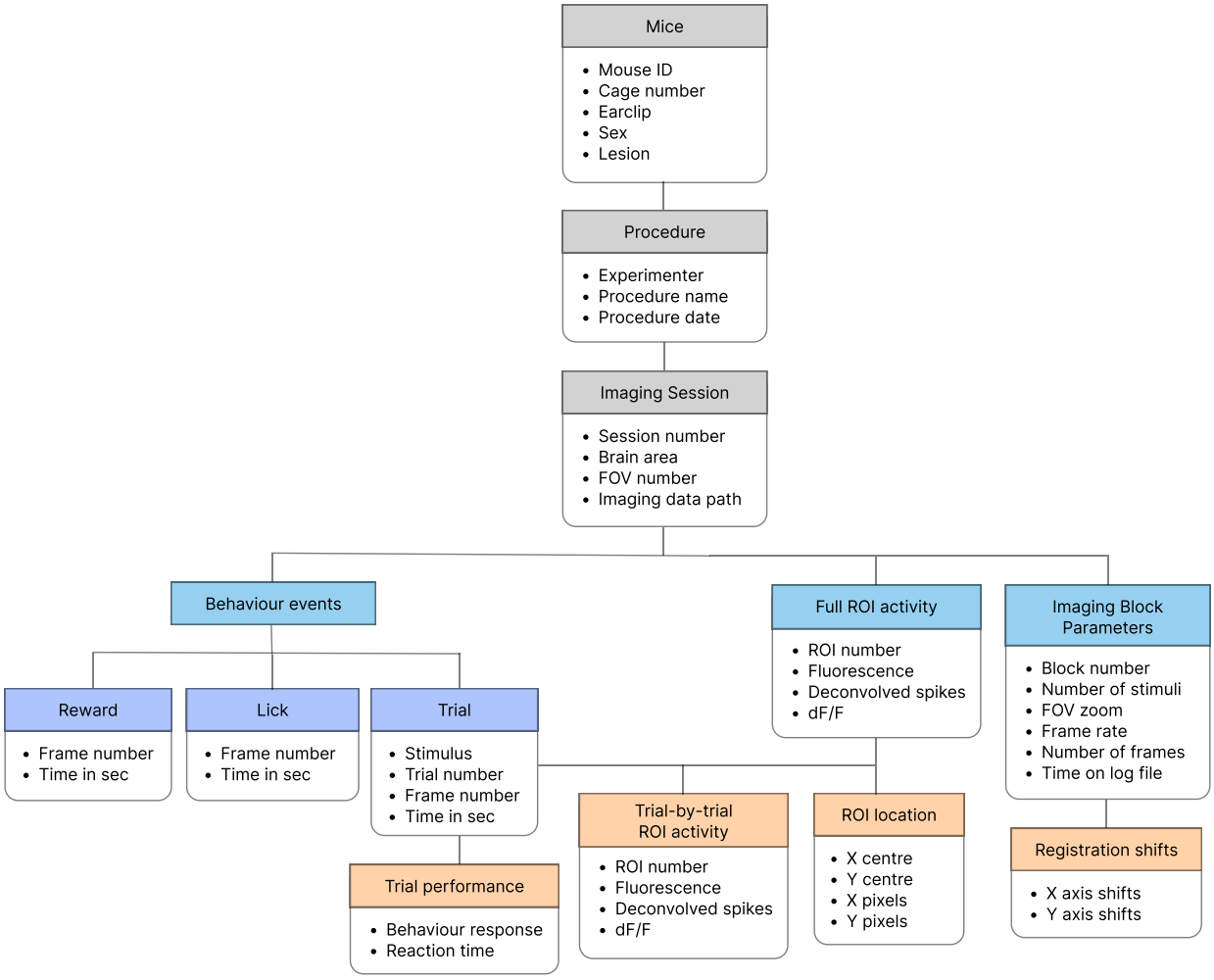

Figure 2.1: Example schema and entity relationship diagram. The structure and and relationship between different tables in an example database developed for this thesis. Each box represents a table, and the bullet points indicate the data stored in a given table. Tables from top to bottom indicate their dependencies - the tables below always depend on the tables above. Colours indicate the type of tables: grey: manual tables, light blue: imported tables, dark blue: part tables, orange: computed tables. ROI: region of interest, FOV: field of view.

- Imported: Data are transformed and automatically ingested into the tables, but require access to external data sources (e.g. raw text files for behavioural events, preprocessed calcium imaging data).
- Computed: Data are computed using other tables in the database.
- Part: Sub-tables that belong to a "master" table where there is a group of associated data. This ensures all parts of the master table appear together or not at all.

A schema defines the structure of a database. **Figure 2.1** shows an example schema used to store data collected for this thesis.

2.5.2 ETL Pipelines

A data pipeline is a set of actions that are operated on the data, often involving moving data from the source to a destination. One of the common data pipelines is the Extract, Transform, Load (ETL) pipeline, which is a series of steps that extracts data from a source or multiple sources, transforms the data, and then loads them into a destination system, such as a database or a data warehouse.

To maintain an efficient data workflow, I developed ETL pipelines for the raw and preprocessed data, and the intermediate and final results were stored in the relational databases. **Figure 2.1** also represents an entity relationship diagram (ERD), which visualises the design of an example ETL pipeline. Briefly, the information about a given mouse and procedures (e.g. experiment sessions, surgical procedures) were manually entered into the database. Once an imaging session was performed, the associated information such as the brain area imaged and the location of the imaging files were also manually entered. After the manual entries, information about a given imaging session would then be automatically extracted from the file locations specified in the manual tables, and the data would be preprocessed before loading into the database for flexible query to perform further analysis.

Together, by developing databases and data pipelines, I was able to better manage data from multiple sources, flexibly access the preprocessed data, and maintain efficient data processing workflows. The system developed is also beneficial for the long-term data management in the lab.

2.6 Clustering analysis

To identify sub-populations of CRIC neurons with distinct response profiles, clustering analysis was performed on all the neurons recorded after the mice had learned the task, using an approach largely similar to what was described in a previous study (Namboodiri et al. 2019).

Trial-averaged activity

For each neuron, the trial-averaged activity was obtained by averaging across all the sound levels presented in a given session for hit and miss trials, respectively. To concatenate the activity of each neuron across sessions, the activity was linearly interpolated to be the same number of frames (193 frames). The difference in the number of frames across sessions (193 - 197 frames for a trial, which lasted for 7 sec) was a result of differences in the size of the field of view across sessions, which resulted in slight differences in the frame rate and thus frame duration. The trial-averaged activity for hit and miss trials was appended together for each neuron, producing 386 data points (frames) per neuron for a total of 2672 neurons (n = 1697 neurons, 40 sessions for 9 unlesioned mice; n = 975 neurons, 43 sessions for 8 lesioned mice). This high dimensional neural activity (2672 x 386) was projected to a lower dimensional subspace before applying the clustering algorithm (see next section).

Principal component analysis

To reduce the dimensionality of the trial-averaged activity for all the neurons recorded, principal component analysis (PCA) was performed along the time axis to capture the temporal response profile for each neuron. A scree plot showing the fraction of variance explained by each principal component (PC) was employed to determine the number of PCs to use in the clustering algorithm (**Figure A.2a**). The standard method is to find an "elbow" point in the plot, which is the point that shows a sharp decrease in the slope of the variance explained curve, followed by a more gradual decrease in slope, as there is minimal variance explained by each PC beyond this point. The elbow point of the scree plot corresponds to PC 9 (**Figure A.2a**), therefore, the high-dimensional neural activity was projected to the lower dimensional subspace formed by the first 9 PCs. The resulting data were used as the input for the clustering analysis.

Spectral clustering

Spectral clustering was used to cluster the data. The affinity matrix was constructed by computing a graph of nearest neighbours. The hyperparameters of the clustering algorithm, including the number of nearest neighbours and the number of clusters, were optimised by a grid search to maximise the mean Silhouette Score for all samples. The Silhouette Score is a measure of the compactness of individual clusters (intra-cluster distance) and the separation amongst clusters (inter-cluster distance). For a given sample i that belongs to cluster C_I, the Silhouette Score is defined as:

$$s_i = \frac{(b_i - a_i)}{max(a_i, b_i)} \tag{2.5}$$

where a_i is the mean distance between sample i and all the other samples in the same cluster, and b_i is the mean distance of sample i to the nearest cluster that sample i is not part of. Let $|C_I|$ and $|C_J|$ be the number of samples belonging to cluster C_I and C_J, and *d(i, j)* be the distance between samples i and j; a_i and b_i are defined as:

$$a_i = \frac{1}{|C_I| - 1} \sum_{j \in C_I, i \neq j} d(i, j) \tag{2.6}$$

$$b_i = \min_{J \neq I} \frac{1}{|C_J|} \sum_{j \in C_J} d(i, j) \tag{2.7}$$

After the optimal hyperparameters were found, the stability of the clusters was further examined by running the clustering algorithm 20 times with random initial starting points. Rand index (RI) measures the similarity between clustering results by counting the number of pairs of samples that are assigned in the same or different clusters in the predicted and reference clustering results (**Equation** 2.8). Adjusted rand index (ARI) adjusted for chance (**Equation** 2.9), so that the values are close to 0 when the results indicate a random labeling of clusters and 1 when the clustering results are identical. The average adjusted Rand index for the clustering

results computed with 20 random initial starting points is 0.979 (standard deviation: 0.009), indicating that the results across randomisation were very consistent.

$$\textbf{Rand index} = \frac{\mathbf{N}_{\text{agreeing pairs}}}{\mathbf{N}_{\text{pairs}}} \tag{2.8}$$

$$\textbf{Adjusted Rand index} = \frac{\mathbf{RI} - \mathbf{RI}_{\text{expected}}}{\max \mathbf{RI} - \mathbf{RI}_{\text{expected}}} \tag{2.9}$$

2.7 Population decoding

Logistic regression

To understand whether the CRIC network activity represented behaviourally relevant information during stimulus trials, logistic regression was trained on the network activity of each session to classify hit versus miss trials on a trial-by-trial, frame-by-frame basis (i.e., each timepoint of each session was trained separately). For each timepoint of each session, an activity matrix of trials by neurons was fed into the model. Sessions were only included if there were at least 15 instances for both hit and miss trials, which excluded 5 imaging sessions from this analysis (each from a different mouse, 3 lesioned and 2 unlesioned). Each timepoint was an imaging frame, which was 35 - 37 ms in duration depending on the size of the FOV. The neuron models were trained with L2 regularisation, which gave similar contributions to correlated features (i.e., individual neuronal activity) instead of discarding some of the correlated features that were also related to behaviourally-relevant information. For PC models, since the features were by definition uncorrelated, L1 regularisation was used to discard uninformative features. The strength of the regularisation for each model was hyperparameter-tuned and the results reported were cross validated. Specifically, neural data in each session was split into 5 stratified folds, and each fold preserved the percentage of hit and miss trials in a given session. 4 folds were used for cross-validated hyperparameter search (randomized search drawn from the log-uniform distribution between 1×10^{-4} and 1×10^{2}), and the remaining 1

fold was used for evaluating the model after the best found hyperparameters were refitted on the 4 folds of data. To more reliably estimate the model results, this process was repeated 5 times for each session and the average of these 5 results were taken as each session's model performance at each timepoint.

Principal components

Decoding using principal components (PCs) as features was performed in the same way as described in **Logistic regression**, except principal component analysis (PCA) was first performed on the trial-by-trial neural activity before training the models. For each timepoint, a neural activity matrix of trials by neurons was constructed and PCA was performed on the neuron axis. Hence, the resulting PCs could be interpreted as sub-populations of neurons that had similar activity patterns across trials at each timepoint. The PCs were by definition uncorrelated, allowing the exploration of logistic regression coefficients without the problems of collinearity.

Class imbalance

The percentage of hit and miss trials was different in each session, and the number of hit trials were often more than the number of miss trials after the mice were trained. To include as many trials as possible while preventing the models from learning only from the majority class, the following balancing procedures were performed.

Logistic regression was trained with the class weights adjusted inversely proportional to the frequencies of each trial type in the training data, giving higher weights to the minority class and lower weights to the majority class (Equation 2.10). Given the total number of trials in the training data $\mathbf{N}_{\mathrm{T}}$, the number of classes $\mathbf{N}_{\mathrm{C}}$, and the number of trials for a given class $\mathbf{N}_{\mathrm{i}}$, the weight for a given class $\mathbf{W}_{\mathrm{i}}$ was defined as follows:

$$\mathbf{W}_{\mathrm{i}} = \mathbf{N}_{\mathrm{T}}/(\mathbf{N}_{\mathrm{C}} * \mathbf{N}_{\mathrm{i}}) \tag{2.10}$$

These weights were then applied to the cost function during the training process to increase the penalty for minority class misclassifications and reduce the penalty for majority class misclassifications.

To avoid the estimated model performance being inflated due to class imbalance, balanced accuracy (Brodersen et al. 2010) was used to report the model performance. Balanced accuracy was defined as the arithmetic mean of the true positive rate and the true negative rate (Equation 2.11), which prevented apparent "good" model performance if the model was simply predicting the majority class all the time. If the model performed equally well on either class, the balanced accuracy would be the same as the conventional accuracy (i.e., the number of correct predictions divided by the total number of predictions). However, if the conventional accuracy of the model was above chance only because the model took advantage of the class imbalance, the balanced accuracy would be at chance level. Here, a balanced accuracy of 0.5 is the chance level model performance.

Balanced accuracy

$$= \frac{1}{2} * \left(\frac{\mathbf{N}_{\text{true positive}}}{\mathbf{N}_{\text{true positive}} + \mathbf{N}_{\text{false negative}}} + \frac{\mathbf{N}_{\text{true negative}}}{\mathbf{N}_{\text{true negative}} + \mathbf{N}_{\text{false positive}}}\right) \tag{2.11}$$

Dummy models

Dummy models were used as baseline models to compare against the performance of the logistic regression models. Dummy models predicted the class labels (i.e., hit or miss trials) randomly while taking into account of the probability of each class.

Correlation analysis

To assess whether the model performance was correlated with the number of neurons identified in each session, Spearman's correlation coefficient was computed between the number of neurons identified in each session and the mean model performance for each 1-sec window over the course of a trial.

Session sampling

Since the number of neurons identified in each session was different, and that there was a significant difference between the sessions of lesioned versus unlesioned mice (see Figure 5.1), subsets of sessions were sampled to ensure matched (within ±5% difference) or equal number of neurons between pairs of sessions of lesioned and unlesioned mice. This was to ensure any difference in the model performance found between lesioned and unlesioned mice was not due to the difference in the number of neurons identified. Specifically, for each session of lesioned mice, if there was at least one session of the unlesioned mice that had equal or matched number of neurons, one of the sessions was randomly selected to be included for analysis. Same number of sessions was drawn for lesioned and unlesioned mice.

Model comparisons

Statistical tests were conducted to compare the model performance between lesioned and unlesioned mice, as well as between the trained models and dummy models. Since the frame rates depended on the size of the FOV, there could be different number of frames (193 - 197 frames) included in a trial (7 sec) across sessions. Thus, model performance was linearly interpolated to make all sessions contain the same number of frames before statistical tests were performed at each timepoint. The model performance of each session was cross-validated and averaged across folds (see **Logistic regression**), and the statistical tests were performed on the distributions of the sessions' model performance. Shapiro–Wilk test was used to determine whether a parametric or nonparametric test should be used, using $p < 0.05$ as a criterion. A one-sided Wilcoxon signed-rank test or paired t-test was performed for comparing trained versus dummy models and trained neuron models versus PC models, while a one-sided Mann-Whitney U test or t-test was performed for comparing trained models for lesioned versus unlesioned mice. Since the number of sessions were less in "matched" and "equaled" sessions (see **Selected sessions**), the balanced accuracy scores were binned every two timepoints (frames) to ensure

sufficient numbers of samples for statistical significance. Statistical significance was defined as $p < 0.05$ after Bonferroni correction.

Neuron contributions

To estimate the contributions of each neuron to the performance of PC models, the model coefficients were mapped back to the neuron space. Specifically, for each session, the 5 repetitions of training (see **Logistic regression**) produced 5 coefficients for each feature at each timepoint. These coefficients were averaged and mapped back to the neuron space by taking the dot product of the averaged coefficients and the loadings of the PCs (i.e., the weights of each neuron for each PC). The absolute value of the resulting values were used to estimate each neuron's contribution to the model performance. If the model did not converge during training for any timepoint, a value of 0 would be assigned as the coefficients would be unreliable when models did not converge.

3

Sound detection with and without auditory cortical inputs

Contents

3.1 Learning and performing a sound-guided task with and without AC 36
3.2 Development of optogenetics strategies 38

As detailed in **Chapter 1**, the functional characteristics of the auditory cortico-collicular (CC) pathway are poorly understood, especially in terms of the neural representation during behaviour. To understand the role of this pathway in sound-guided behaviour, measuring neural activity during a sound-guided task while manipulating the AC inputs is required. Here, two-photon calcium imaging was used to measure the activity of auditory cortico-recipient inferior colliculus (CRIC) neurons while mice learned and performed a sound detection task. Both chronic and acute inactivation of AC inputs was attempted as complementary approaches, conducted by either permanent lesions of the AC (Chapter 3.1) or transient optogenetic inactivation of the CC axons in the IC (Chapter 3.2). For technical reasons, the effect of optogenetic silencing of CC axons in the IC remains unclear, but the process of developing the optogenetics strategy is detailed in Chapter 3.2.

3.1 Learning and performing a sound-guided task with and without AC

To selectively measure the activity of CRIC neurons, an adeno-associated virus (AAV)-mediated anterograde transsynaptic approach (Zingg et al. 2017) was used to express Cre in transgenic mice (Ai95D) that Cre-dependently expressed GCaMP6f (see **Intracranial injection** in 2.1). **Figure 3.1a** shows an example image of the GCaMP6f-expressing CRIC neurons. To assess the effect of AC inputs on the neural activity of CRIC neurons and behaviour, the AC was chronically removed bilaterally by either aspiration (Hong et al. 2018) or thermo-coagulation (Ceballo et al. 2019) in 8 out of 17 mice (see **Cortical lesions** in 2.1). **Figure 3.1b,c** shows the extent of the bilateral AC lesions for an example mouse.

To investigate the activity of CRIC neurons during behaviour and how it changes when AC inputs are removed, mice were trained daily to report a 0.5 ms broadband click stimulus by licking within a response window to obtain a water reward (**Figure 3.2a**). **Figure 3.2b** shows the possible behavioural outcomes of a trial. An automated behavioural training pipeline was developed to ensure the reproducibility of training across mice (**Figure 3.2c**)[1]. To train naïve mice to associate the stimulus with a water reward, the sound was presented at 80 dB sound pressure level (SPL) followed by the delivery of a water reward during the initial passive training phase. If the mouse successfully responded for 3 consecutive trials, it would transition into the active training phase for the rest of the session, where the mouse had to lick within the respond window to trigger a water reward in stimulus trials (**Figure 3.2c**). After the mouse had learned the task, stimuli with lower sound levels were introduced to introduce uncertainty to the task (**Figure 3.2c**).

Mice with bilateral AC lesions ("lesioned mice") were able to learn and perform the sound detection task, and there was no significant difference between the

[1]Experiments conducted by colleagues started with the active training phase directly and did not use the automated behavioural training pipeline. If the mouse did not respond to the stimulus, rewards were delivered manually at times based on colleagues' judgements.

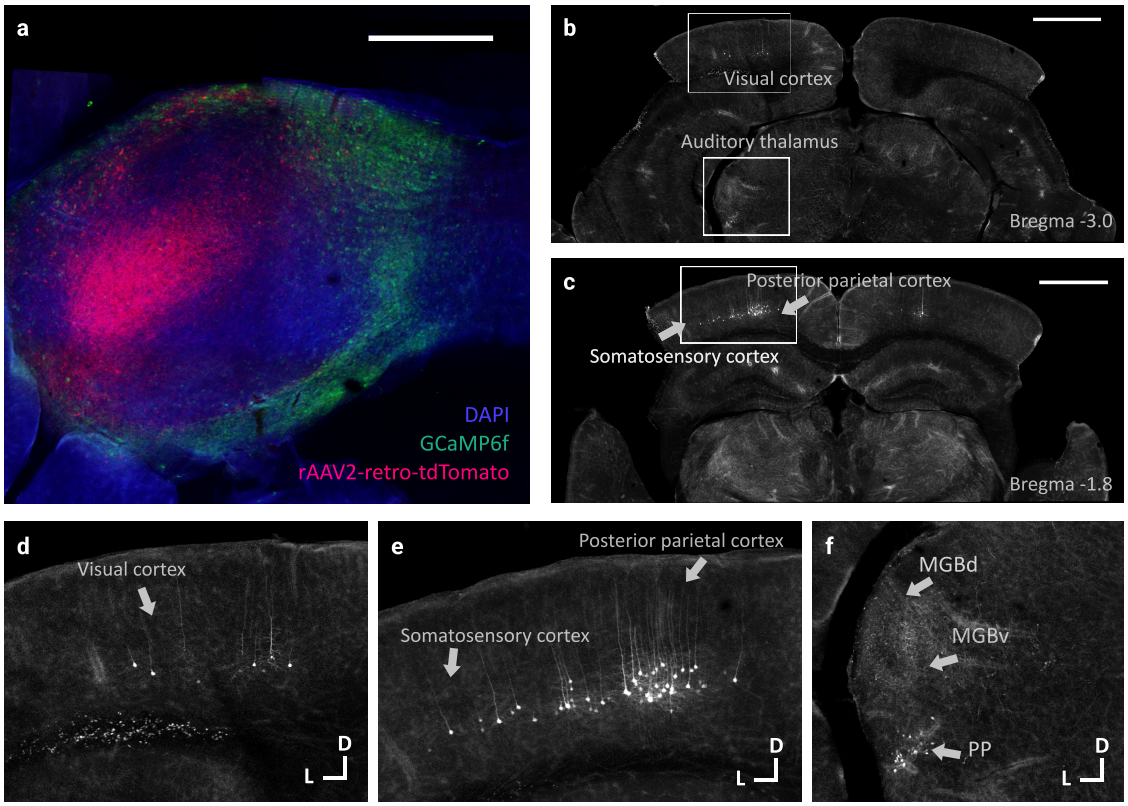

Figure 3.1: Expression of GCaMP6f, lesion sites, and rAAV2-retro tracing. **(a)** Injection of AAV1-hSyn-Cre in the AC of Ai95D mice selectively drove the expression of GCaMP6f (green) in neurons in the shell of the IC that receive AC inputs. Injection of rAAV2-retro-tdTomato (red) into the dorsal IC labelled neurons in the central nucleus of the IC and other cortical and thalamic neurons (b-f) that project to the dorsal IC. Scale bar: 500 µm. **(b-c)** Coronal sections showing the extent of the bilateral auditory cortical lesions, and the retrogradely labelled IC-projecting neurons in the visual, somatosensory, and posterior parietal cortices as well as the auditory thalamus. No tdTomato-positive neurons were found near the edge of the lesions, suggesting that the part of the AC that projects to the dorsal IC had been removed. Scale bar: 1 mm. **(d-f)** Magnified versions of the areas indicated by white rectangles in (b-c) showing IC-projecting neurons in the visual (d), somatosensory, and posterior parietal cortices (e), as well as the peripeduncular nucleus (PP) of the auditory thalamus (f). L: lateral; D: dorsal; MGBd: dorsal division of the medial geniculate body; MGBv: ventral division of the medial geniculate body.

behavioural performance of lesioned mice and those without AC lesions ("unlesioned mice") for the 80 dB SPL stimulus across days ($p > 0.05$ for the "lesion" factor and $p < 0.001$ for the "day" factor, mixed-design ANOVA) (**Figure 3.2d,f**). Additionally, the behavioural performance of both lesioned and unlesioned mice improved significantly as the sound level of the stimulus increased ($p < 0.001$ for the "sound level" factor, mixed-design ANOVA), and there was no significant difference between them in their ability to detect stimuli of different sound level categories ($p > 0.05$ for the "lesion" factor, mixed-design ANOVA) (**Figure 3.2e,g**). These results suggested that mice were able to learn and perform the sound detection task regardless of the presence of the AC, and there was no significant difference in their ability to learn across days and to detect stimuli of different sound levels.

3.2 Development of optogenetics strategies

The previous section showed that mice without an AC in each hemisphere were able to learn and perform the sound detection task as well as mice with intact AC. Another approach to study the CC pathway and its influence on the IC is to acutely inactivate the CC axons in the IC with optogenetics. While lesions are permanent and unspecific, optogenetic approaches would enable the selective and reversible manipulation of the CC pathway, with the temporal precision to study its effect on specific task variables in a trial. Seven different viral strategies were attempted during the technical development of the optogenetics experiments (**Table 3.1**). However, the effect of optogenetic silencing of AC axons on mouse behaviour and the responses of IC neurons remain inconclusive. The technical development of this approach is documented in this section.

To inhibit CC axons while imaging CRIC neurons, AAV1-hSyn-Cre and the Cre-dependent inhibitory opsin, AAV8-FLEX-Jaws-tdTomato, were injected into the AC of the Ai95D transgenic mice. This approach should result in the expression of GCaMP6f in CRIC neurons as well as the expression of Jaws in AC neurons and axons, including CC axons. The hope was that this would enable us to manipulate the AC inputs to the IC while imaging CRIC neurons. To assess how silencing AC

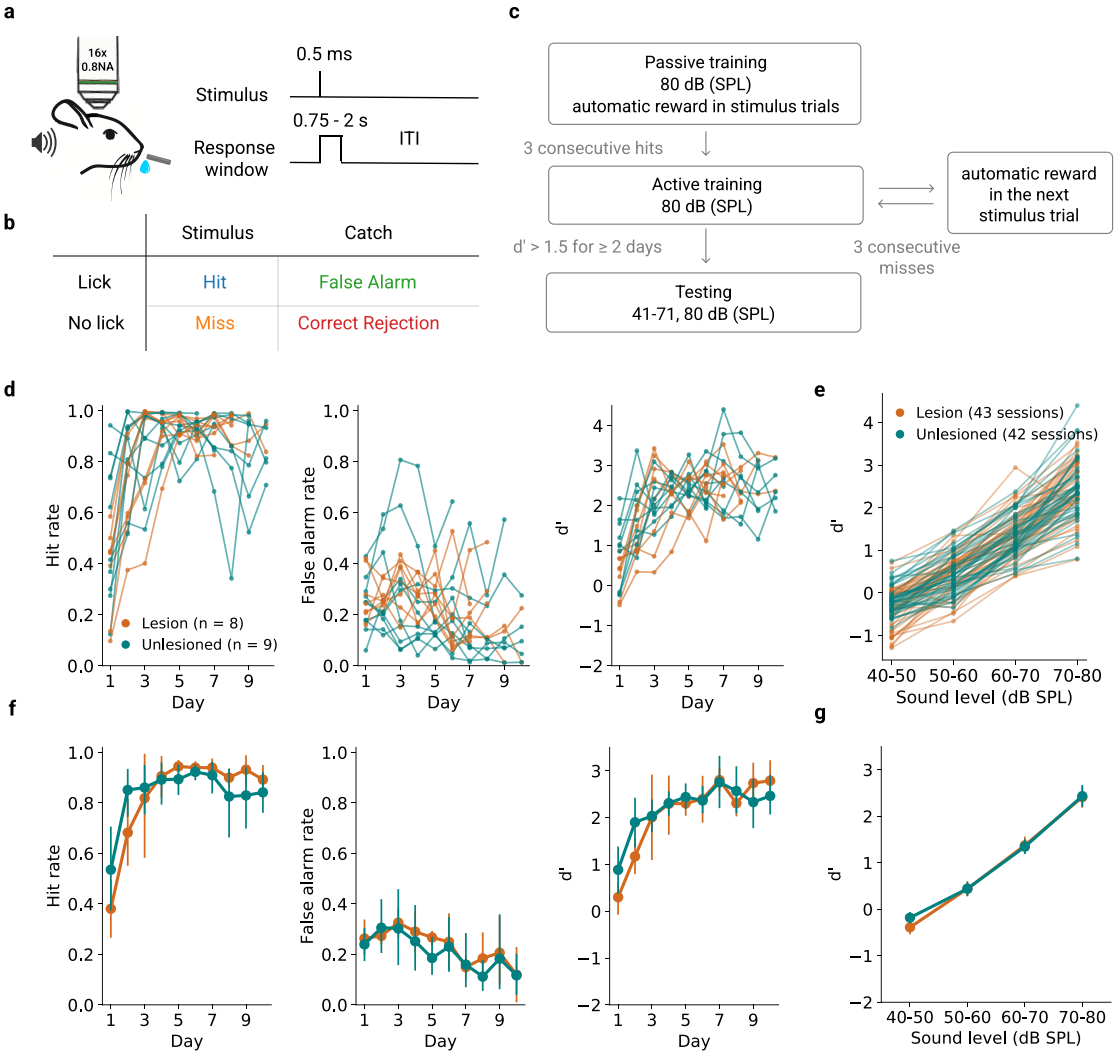

Figure 3.2: Mice learned and performed the sound detection task regardless of the presence of the AC. (a) The structure of the sound detection task. Mice were trained to report a 0.5 ms broadband click stimulus by licking within the response window to trigger a water reward. Neural activity was recorded with two-photon calcium imaging while the mice learned and performed the task. ITI: inter-trial interval. **(b)** Stimulus conditions and possible behavioural outcomes of a trial. No stimulus was presented in catch trials. **(c)** Structure of the behavioural training and testing. **(d)** Individual mouse's performance for the 80 dB (SPL) stimulus across days. Note the number of days were not necessarily the same across mice. **(e)** Psychometric curves of different sound intensities for each session during the testing phase. **(f)** Same as **(d)** but averaged across mice. Behavioural performance for the 80 dB SPL stimulus in both lesioned and unlesioned mice improved significantly over time ($p < 0.001$, mixed-design ANOVA), and there was no significant difference between the behavioural performance of lesioned and unlesioned mice ($p > 0.05$, mixed-design ANOVA). **(g)** Same as **(e)** but averaged across mice. Behavioural performance significantly improved as the level of the stimulus increased ($p < 0.001$, mixed-design ANOVA), while there was no significant difference between the behavioural performance of lesioned and unlesioned mice ($p > 0.05$, mixed-design ANOVA). Error bars indicated 95% confidence intervals.

inputs influences the activity of CRIC neurons, pure tones were presented to the mice while optogenetic laser stimulation was delivered over the dorsal IC in half of the trials, with the aim to inhibit AC axons in the IC. There was no difference between laser on and laser off condition in the responses of CRIC neurons to their best frequency (BF, the sound frequency that evoked the strongest response of a neuron) (**Figure 3.3c**, left) ($p > 0.05$, Wilcoxon signed-rank test, 10/149 responsive neurons, 3 mice). Furthermore, when the histological images were examined, no tdTomato-labelled neurons could be identified. This was consistent across 6 mice, suggesting that this viral approach was unsuccessful. Thus, the experiments were repeated and the opsin was replaced by AAV5-hSyn-eNpHR3.0-mCherry. Optogenetic laser stimulation of the AC axons showed no effect on the responses of CRIC neurons to their best frequencies (**Figure 3.3c**, middle) ($p > 0.05$, Wilcoxon signed-rank test, 32/103 responsive neurons, 4 mice). Since it was difficult to establish whether silencing axons had no effect on the responses of CRIC neurons or whether the opsins were dysfunctional, the same experiments were repeated with another virus, AAV1-Flex-Jaws-tdTomato. Optogenetic laser stimulation of AC axons appeared to result in a small decrease in the responses of CRIC neurons to their best frequencies (**Figure 3.3c**, right) ($p < 0.05$ ($p = 0.04584$), Wilcoxon signed-rank test, 125/495 responsive neurons, 6 mice). However, histological images showed no identifiable AC neurons or axons labelled with AAV1-flex-jaws, tagged with tdTomato. This was consistent across 8 mice examined with confocal microscopy, of which 2 were injected bilaterally. While it was possible that this opsin was expressed while the tdTomato was not, when injecting AAV1-flex-jaws into Rbp4-Cre transgenic mice, which allowed the expression of this construct in Rbp4-positive neurons of the AC (targeting mostly layer 5 in the cortex), tdTomato was clearly expressed in neurons in the AC and their axons in the IC (**Figure 3.4**). The Rbp4-Cre mice were injected with both AAV1-flex-jaws and AAV1-Syn-GCaMP6s in the AC, with the aim of imaging and silencing AC axons in the IC to assess the consequences of silencing AC axons. However, due to a hardware malfunction, which took two months to resolve, this experiment was not performed.

Table 3.1: Development of viral strategies for the optogenetics experiments. Seven combinations of viruses and transgenic lines were attempted during the technical development of the optogenetics experiments. The full name of the viruses and transgenic mice could be found in Chapter 2.1. *8 of the mice were used early in the development for setting up the required hardware and software for the optogenetics experiments.

Virus 1	Site 1	Virus 2	Site 2	Mouse line	Number
AAV1-hSyn-Cre	AC	AAV8-flex-jaws	AC	Ai95D	14*
AAV1-hSyn-Cre	AC	AAV5-hSyn-eNpHR3.0	AC	Ai95D	4
AAV1-hSyn-Cre	AC	AAV1-flex-jaws	AC	Ai95D	8
AAV1-Syn-GCaMP6s	AC	AAV1-flex-jaws	AC	Rbp4-Cre	4
-	-	AAV1-flex-jaws	AC	CaMKIIα-Cre-GCaMP6f	3
AAV1-Syn-GCaMP6f	IC	AAV1-flex-jaws	AC	CaMKIIα-Cre-3487	3
AAV1-Syn-GCaMP6f	IC	AAV1-flex-jaws	AC	Rbp4-Cre	3

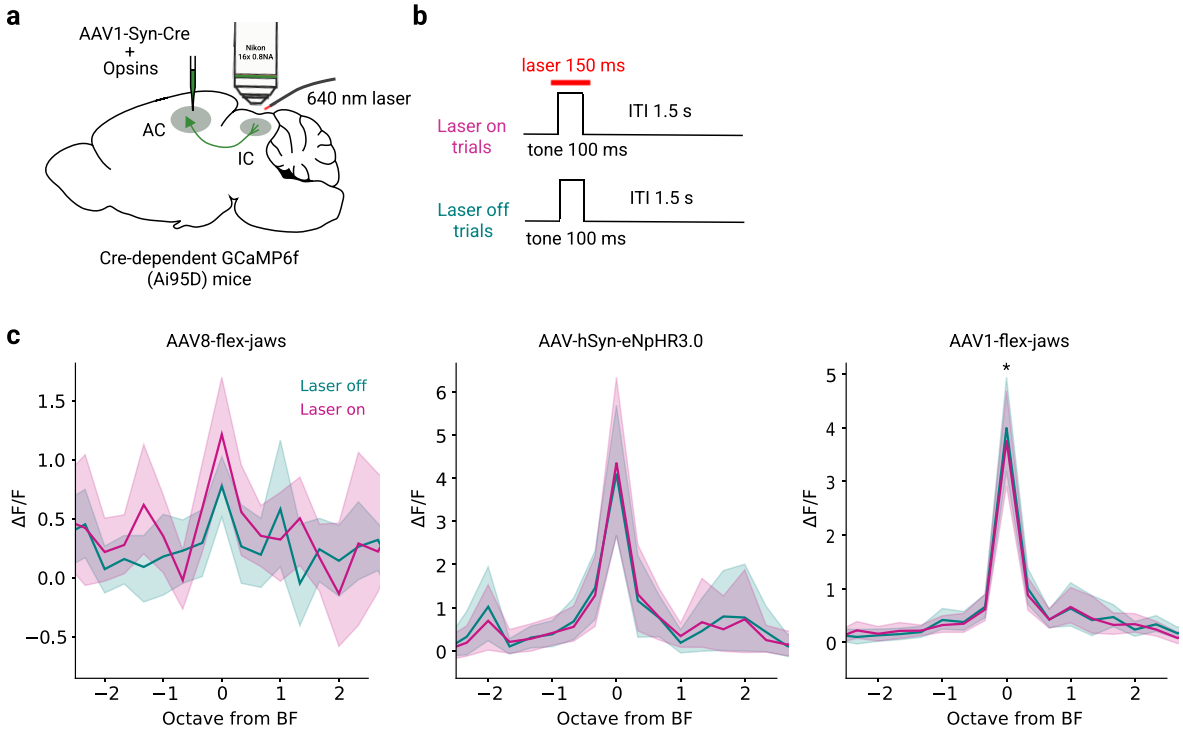

Figure 3.3: Responses of CRIC neurons during optogenetic inactivation of cortico-collicular axons in the IC. (a) Schematic showing the injection strategy. AAV1-Syn-Cre was mixed with opsins and injected into the AC of Ai95D mice. CRIC neurons were imaged with a two-photon microscope and the AC axons in the IC were optogenetically silenced with a 640 nm laser. **(b)** The structure of the tone presentation with optogenetic laser stimulation. ITI: inter-trial interval. **(c)** Responses of responsive CRIC neurons to optogenetic inactivation of CC axons in the IC using different opsins: AAV8-flex-jaws (left), AAV-hSyn-eNpHR3.0 (middle), and AAV1-flex-jaws (right). BF: best frequency; *: $p < 0.05$ ($p = 0.04584$), one-sided Wilcoxon signed-rank test.

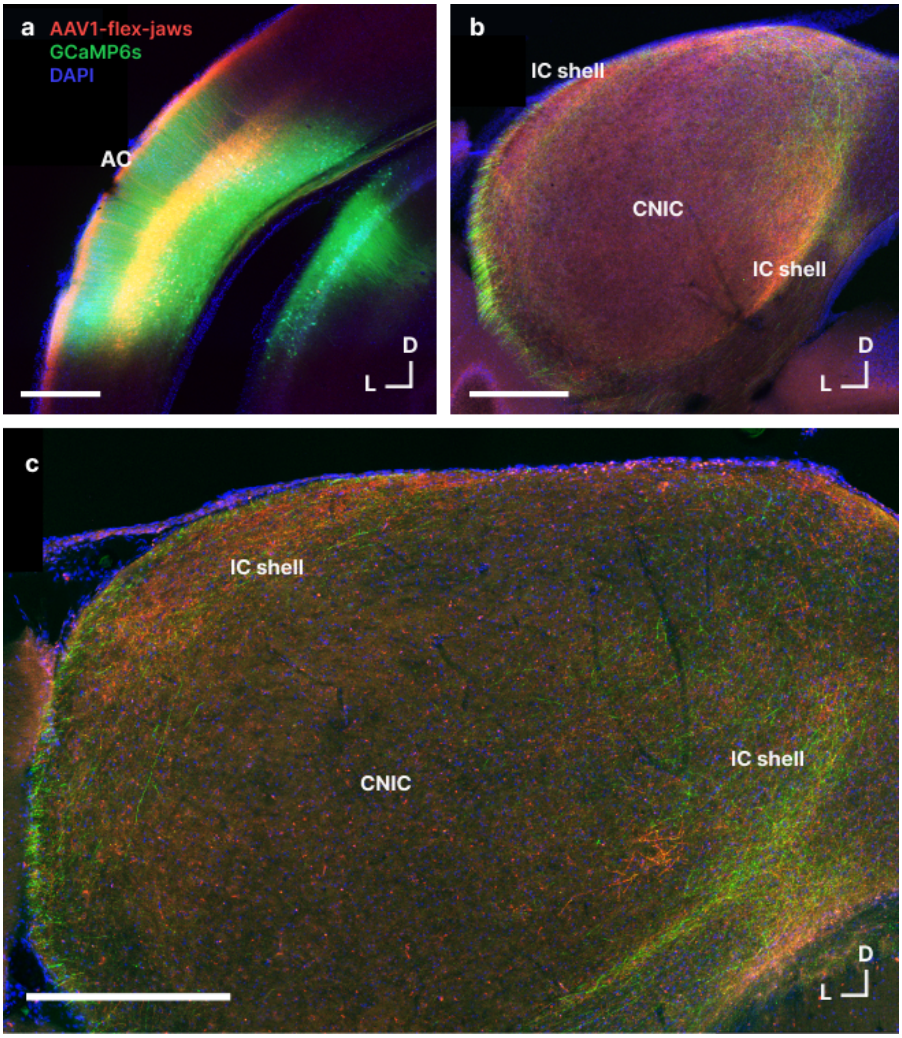

Figure 3.4: Expression of AAV1-flex-jaws and GCaMP6s in the AC and IC of Rbp4-Cre mice. (a) Expression of AAV1-flex-jaws and AAV1-Syn-GCaMP6s in the AC. **(b-c)** AC axons were labelled with AAV1-flex-jaws (red) and AAV1-Syn-GCaMP6s (green) in different rostro-caudal areas of the IC. AC: auditory cortex, IC: inferior colliculus, CNIC: central nucleus of the inferior colliculus. L: lateral; D: dorsal. Scale bars: 500 µm.

Since combining AAV1-flex-jaws with transgenic mice that express Cre showed expression of the opsin in the AC neurons and axons, while combining this opsin with AAV1-hSyn-Cre injections did not, the former strategy appeared to be the way forward.

Research has shown that CaMKIIα expresses in neurons in the IC and AC (Wang et al. 2013), therefore, expressing AAV1-flex-jaws in the AC of transgenic mice that expresses CaMKIIα-Cre and Cre-dependent GCaMP6f would allow us to silence axons of CaMKIIα-positive AC neurons, including CC neurons, while imaging

CaMKIIα-positive IC neurons. Even though this strategy lacks the advantage for imaging CRIC neurons specifically, it would allow us to examine the effect of silencing AC axons on IC neurons in general. One caveat is that the expression of CaMKIIα-Cre may be too sparse in the IC, which would result in low number of neurons that could be imaged per field of view. Indeed, when examining the GCaMP6f expression with two-photon microscopy, 4 out of 6 mice (3 of which did not have opsins injected) did not show sufficient expression of GCaMP6f in the IC. Therefore, this approach was not pursued further. Another option was to inject GCaMP6f in the IC and AAV1-flex-jaws in the AC of suitable transgenic mice that expresses Cre.

Therefore, AAV1-Syn-GCaMP6f was injected into the IC and AAV1-flex-jaws into the AC of two Cre-driver lines: CaMKIIα-Cre-3487 and Rbp4-Cre mice. However, the Cre expression in the CaMKIIα-Cre-3487 line turned out to be mosaic Golgi-staining-like pattern (Chakravarthy et al. 2006), which was not suitable as only few AC axons would be labelled and thus be inhibited in the IC, making it difficult to assess how silencing AC inputs influences the activity of IC neurons. Therefore, two-photon calcium imaging experiments were performed on Rbp4-Cre mice only. Optogenetic inhibition of AC axons showed no effect on the responses of IC neurons to their best frequencies in the Rbp4-Cre mice (**Figure 3.5b**) ($p > 0.05$, Wilcoxon signed-rank test, 76/454 responsive neurons, 3 mice).

Possible reasons for this result include not being able to sufficiently activate the opsins or to inhibit a large enough population of axons. Due to lack of specificity for the expression of GCaMP6f in the Rbp4-Cre mice, it is also possible that some of the neurons recorded do not receive AC input, thus were not directly influenced by the silencing of AC axons. Another possibility is that optogenetic silencing of the auditory CC pathway has no effect on IC responses during passive listening conditions (Blackwell et al. 2019). Therefore, the 3 Rbp4-Cre mice injected with AAV1-Syn-GCaMP6f and AAV1-flex-jaws were trained to perform the sound detection task described in the previous section (**Figure 3.2a**). The structure of the task was the same as described in (**Figure 3.2a-c**), except that during the training phase, the optogenetic laser stimulation was present in all the trials

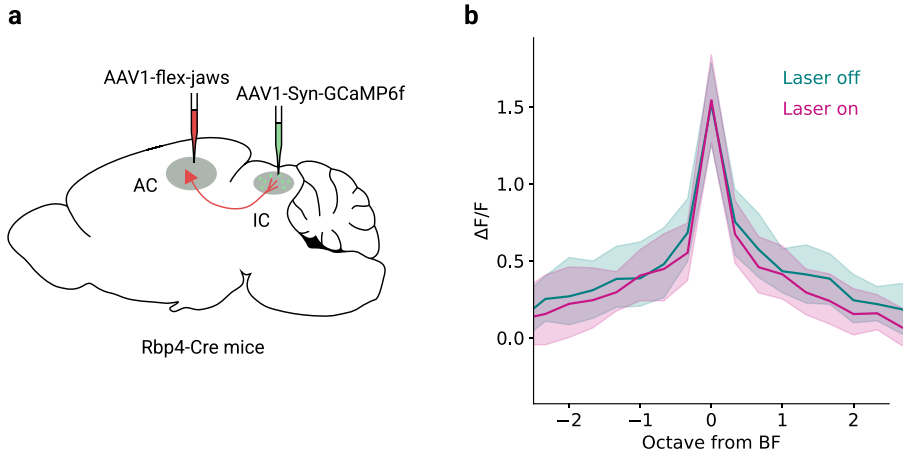

Figure 3.5: Responses of IC neurons during optogenetic inactivation of cortico-collicular axons in the IC. (a) Schematic showing the injection strategy. AAV1-flex-jaws was injected into the AC and AAV1-Syn-GCaMP6f was injected to the IC of Rbp4-Cre mice. IC neurons were imaged with a two-photon microscope and the AC axons in the IC were optogenetically silenced with a 640 nm laser as illustrated in **Figure 3.3a**. **(b)** Responses of responsive IC neurons to optogenetic inactivation of cortico-collicular axons in the IC. BF: best frequency.

to assess whether inhibiting cortico-collicular axons influences learning. In the subsequent testing phase where multiple sound levels were presented, the clicks were paired with laser stimulation in all the trials in early sessions and in around 50% of the trials in later sessions. 2 of the 3 mice learned the task within the first day (**Figure 3.6a**, left), while the remaining mouse did not learn the task (d prime < 1.5) after 3 consecutive days of training. The cranial window of this mouse was covered with blood from the 4th day of training for at least 3 days, making it difficult to optogenetically stimulate the axons and image the neurons. Thus, no further experiment was performed with this mouse.

After two days of training, clicks were paired with laser stimulation in 50% of the trials in later sessions to assess the effect of silencing cortico-collicular axons on IC responses and the mouse's behaviour on a trial-by-trial basis. The performance of the mouse was significantly better as the stimulus sound levels increased ($p < 0.01$, two-way ANOVA), and there was no significant difference between laser conditions ($p > 0.05$, two-way ANOVA) (**Figure 3.6a**, right). There was also no significant difference in the mouse's reaction time between laser conditions across all the sound level categories (**Figure 3.6b**, $p > 0.05$, one-sided Mann-Whitney U

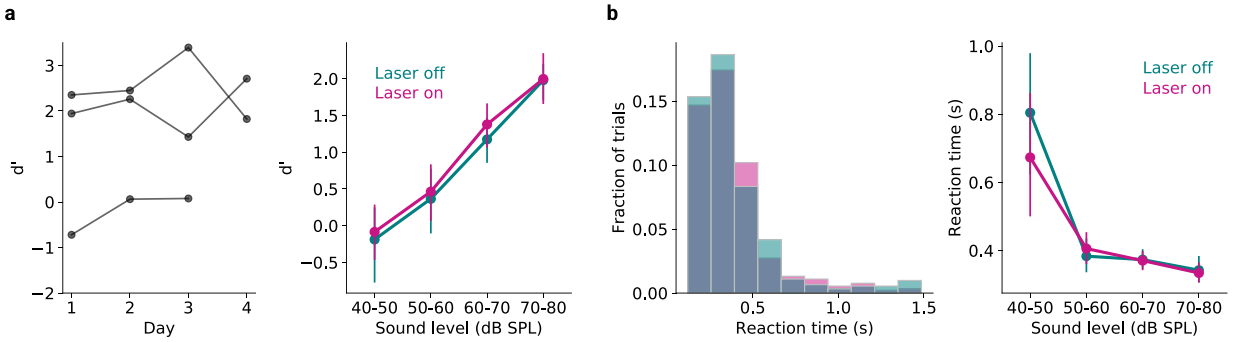

Figure 3.6: Behaviour performance during optogenetic inactivation of cortico-collicular axons. (a) Left: Behaviour performance of 3 Rbp4-Cre mice on the sound detection task for the 80 dB (SPL) stimulus across days. Optogenetic laser stimulation was present in all the trials. Right: Psychometric curves of different sound levels during the testing phase. Optogenetic laser stimulation was present in around 50% of the trials. **(b)** Left: Reaction time distribution during the testing phase (912 hit trials). Right: Reaction time for each sound level category.

test, 912 hit trials, 6 sessions, 2 mice). Analysis is still being done to determine if the laser stimulation had any influence on the responses of IC neurons, but data from more mice would be required to fully assess the effect.

In summary, optogenetic inhibition of AC axons in the IC showed no effect on the responses of IC neurons to their best frequencies in Rbp4-Cre mice. Preliminary data from 3 Rbp4-Cre mice showed that 2 out of 3 mice could learn the sound detection task when the optogenetic laser stimulation was paired with the stimulus. There was no significant difference between laser on vs off conditions for the mice's behavioural performance and reaction time across sound levels. Due to the low number of mice and the uncertainty of the effectiveness of optogenetic stimulation, it remains unclear if optogenetic silencing of cortico-collicular axons resulted in changes in IC responses and behaviour. Therefore, the following chapters focus on studying the responses of CRIC neurons during the sound detection task, and how their neural representation changes when the AC inputs were chronically removed.

4

Heterogeneous response dynamics of the CRIC neurons

Contents

4.1 Temporal profiles of average CRIC population response during sound-guided behaviour 47

4.2 Heterogeneity of individual CRIC neuronal response patterns during sound-guided behaviour 49

As outlined in **Chapter 1**, previous studies have shown that manipulating the activity of the AC results in changes in IC neuron responses (Yan and Suga 1998, Zhang and Suga 2000, Ma and Suga 2001b, Yan et al. 2005, Suga et al. 2002, Yan and Ehret 2002, Ma and Suga 2001a, Nakamoto et al. 2008). However, most research has studied the central nucleus of the IC during passive listening conditions, whereas the cortico-collicular axons terminate mostly in the shell of the IC and might play a different role during behaviour. Therefore, the influence of the AC on the responses of cortico-recipient IC (CRIC) neurons during behaviour remains an open question. As shown in **Chapter 3**, mice could learn and perform a sound detection task when the AC was chronically removed. This chapter characterises the activity of CRIC neurons during behaviour and how it changes when the AC inputs are absent.

4.1 Temporal profiles of average CRIC population response during sound-guided behaviour

To investigate the activity of CRIC neurons during behaviour, GCaMP6f was selectively expressed in CRIC neurons utilising an adeno-associated virus (AAV)-mediated anterograde transsynaptic approach (Zingg et al. 2017) (**Figure 4.1a,b**). In 8 out of 17 mice, bilateral AC lesions were performed so that the effect of AC inputs on CRIC neuronal responses could be assessed. Two-photon calcium imaging was used to record the activity of CRIC neurons while mice learned and performed a sound detection task (**Figure 3.2a**, **4.1c**).

To illustrate the response profiles of the CRIC neuronal population during behaviour, **Figure 4.1d** shows the average responses across all neurons and sessions for each stimulus and behaviour trial type after the mice had learned the task (n = 1697 neurons, 40 sessions for 9 unlesioned mice; n = 975 neurons, 43 sessions for 8 lesioned mice). Qualitatively, stimulus trials (hit and miss trials) were associated with a sharp increase of neural activity immediately following stimulus onset across all the sound levels in both lesioned and unlesioned mice. Such activity was absent in catch trials where no stimulus was presented (**Figure 4.1d**). In hit but not miss trials, the initial sound-evoked responses were followed by a prolonged period of increased activity for at least 3-4 seconds after stimulus onset. This was observed in both lesioned and unlesioned mice, even though their temporal response profiles appeared to be different (**Figure 4.1d**). In the first 2 seconds after stimulus onset, the responses of hit trials in lesioned mice showed an initial increase followed by a decrease before a second peak. This was consistent for stimulus trials of 50-80 dB (SPL) and was not observed in unlesioned mice, implying that the lack of AC might be contributing to this response pattern. The sustained activity observed in both unlesioned and lesioned mice could represent information that was present in hit trials but not miss trials, including the mouse's choice, motor-related activity, or reward.

Taken together, the average CRIC population response across all recorded neurons and sessions exhibited sound-evoked activity in stimulus trials, and the

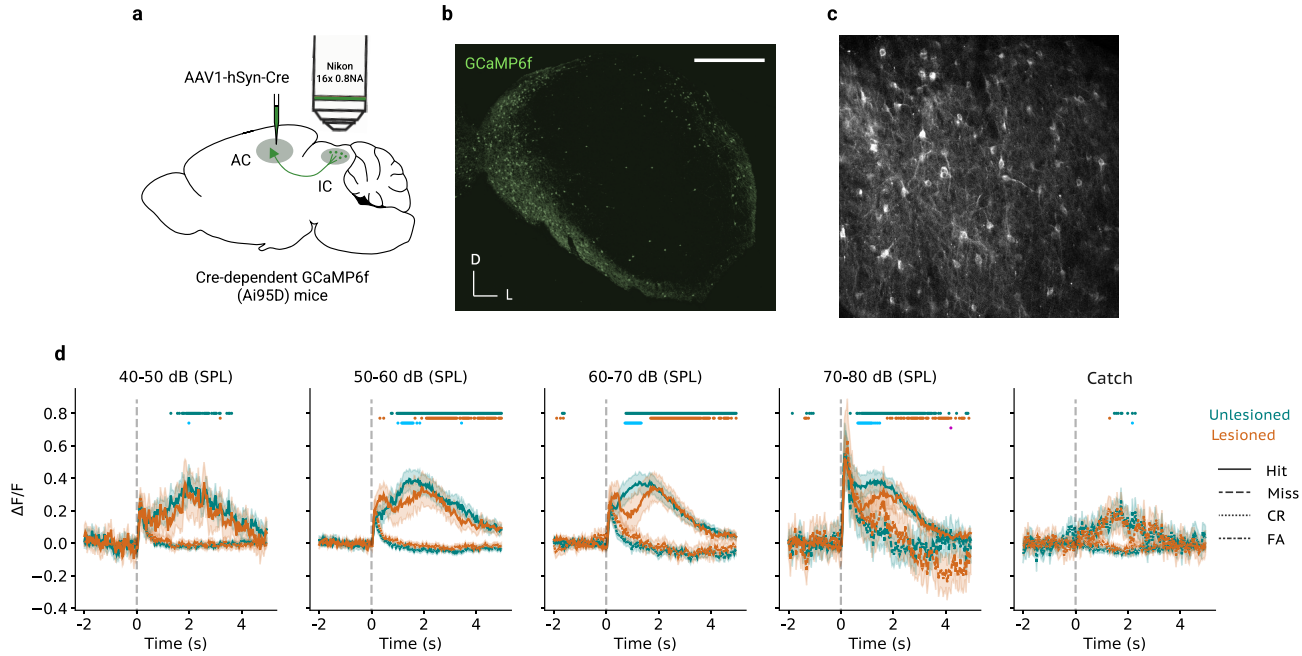

Figure 4.1: Average population response time course for each trial type. **(a)** Schematic showing the viral strategy for labelling and imaging CRIC neurons. **(b)** Example histological image showing the GCaMP6f labelling of CRIC neurons. Scale bar: 500 µm. **(c)** Example imaging field of view (500 x 500 µm). **(d)** Average responses across all neurons and sessions for each stimulus and behaviour trial type (see **Figure A.1** for the plot displaying each trial type separately). The responses of each neuron were baseline-corrected to the mean activity during the pre-stimulus period. The teal and orange dots above the traces indicate the timepoints where the responses of hit or false alarm trials are significantly different from miss or correct rejection trials for unlesioned (teal) and lesioned (orange) mice, while the blue and purple dots indicate significant difference between lesioned and unlesioned mice for hit (blue) and miss (purple) in stimulus trials or false alarm (blue) and correct rejection (purple) in catch trials. Shapiro–Wilk test was used to determine whether a parametric or nonparametric test should be used, using $p < 0.05$ as a criterion. A one-sided Wilcoxon signed-rank test or paired t-test was performed for comparing hit versus miss trials and false alarm versus correct rejection trials, while a one-sided Mann-Whitney U test or t-test was performed for comparing the responses of lesioned versus unlesioned mice. Statistical significance was defined as $p < 0.05$ after Bonferroni correction. CR: Correct rejection. FA: False alarm.

sustained increase in activity was only observed if the mouse successfully reported the detection of the stimulus. These temporal characteristics could be seen even when the AC inputs were absent (albeit with different response patterns), indicating that the average CRIC population response contained behaviourally-relevant information even without inputs from the AC.

4.2 Heterogeneity of individual CRIC neuronal response patterns during sound-guided behaviour

To what extent the observed CRIC population response (**Figure 4.1d**) reflects the response profiles of individual neurons remains unclear. To gain insights into the heterogeneity of response patterns among individual CRIC neurons, an unsupervised clustering approach was employed to identify neurons with different response profiles from both lesioned and unlesioned mice (Namboodiri et al. 2019, see **Clustering analysis**). This allows us to examine if there are any differences in the response dynamics between lesioned and unlesioned mice, which would implicate the invovelment of the AC. For instance, if certain response patterns could only be seen in mice with AC inputs, it would indicate that the AC is involved in influencing those response profiles in the CRIC neurons. Additionally, if there were patterns of responses that were unique to neurons from lesioned mice, it would imply that the CRIC neurons developed those response dynamics following AC lesions.

To perform the clustering analysis, trial-averaged activity of each neuron was obtained by averaging across all the sound levels presented in a given session after the mice had learned the task. This yielded high-dimensional data with 386 time points per neuron for 2672 neurons across lesioned and unlesioned mice. Principal component analysis (PCA) was performed to reduce the dimensionality of these data along the time axis to capture the temporal profile of each neuron, and the data were projected onto the lower dimensional subspace formed by the principal components (PCs) before inputing to the spectral clustering algorithm (**Figure**

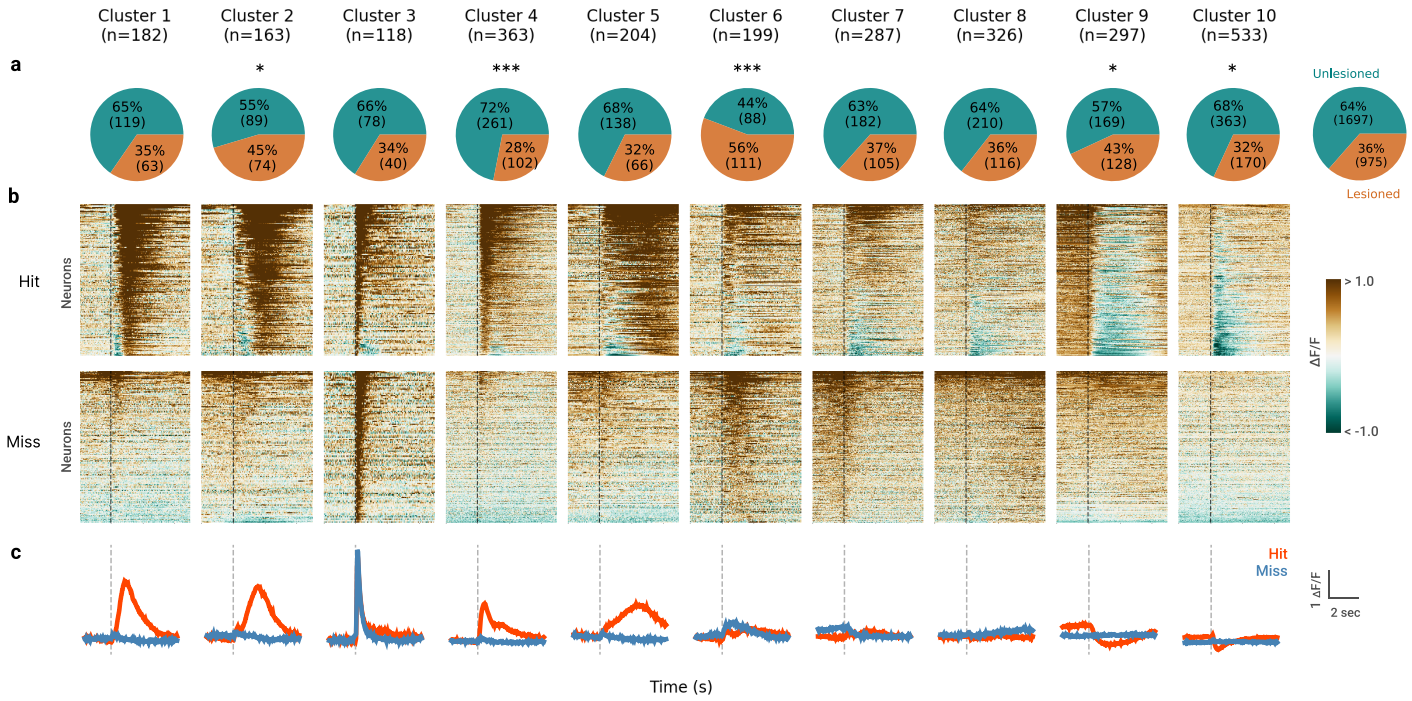

Figure 4.2: CRIC neurons displayed heterogeneous response patterns. (a) Pie charts displaying the number and percentage of neurons from lesioned vs unlesioned mice in a given cluster. Asterisks indicate significant difference between the proportion in the given cluster and the proportion in the overall population. *: $p < 0.05$, **: $p < 0.01$, ***: $p < 0.001$, two-sided one proportion Z-test. **(b)** Individual neuronal response profiles for each identified cluster. Each column represents a cluster. Neurons were sorted separately based on their activity in hit and miss trials. Dashed vertical lines indicate stimulus onset. **(c)** Mean response profile of each cluster. Note that the hit and miss trials in cluster 3 had the same mean amplitude and shape immediately following stimulus onset, thus the traces overlapped. **Figure A.3** displays the responses of neurons from unlesioned and lesioned mice separately.

A.2). This approach revealed 10 clusters of neurons displaying different response patterns over the course of a trial (**Figure 4.2**).

The responses of cluster 3 resembled the sound-evoked responses seen in **Figure 4.1d**, where there was increased activity immediately following stimulus onset in both hit and miss trials. The sustained increased activity seen in hit but not miss trials (**Figure 4.1d**) could also be seen in clusters 1, 2, and 5 with different temporal profiles. There were also other interesting response patterns that could not be seen in the average population response observed in **Figure 4.1d**. For example, cluster 4 showed increased activity immediately following stimulus onset in hit but not miss trials, and the increased activity lasted longer than that observed

in cluster 3. Cluster 10 showed a suppression of activity following stimulus onset in hit but not miss trials. Cluster 6 and 7 exhibited similar temporal dynamics in hit trials, while in miss trials, there was increased activity following stimulus onset in cluster 6 and, interestingly, before stimulus onset in cluster 7. Cluster 9 also displayed positive responses before the stimulus, followed by a sustained suppression after stimulus onset in hit trials. This was only observed in hit but not miss trials. Given that there were no cues before the stimulus and that the inter-trial interval was variable in this behavioural task, the pre-stimulus activity in cluster 7 and 9 could imply the state of the network that is associated with the mouse's successful detection of the upcoming stimulus.

Overall, the CRIC neurons displayed heterogeneous response profiles during behaviour in both lesioned and unlesioned mice, even though the proportions of neurons from lesioned and unlesioned mice in some clusters were different from the proportions in the overall population, including cluster 2, 4, 6, 9 and 10 ($p < 0.05$, two-sided one proportion Z-test). This indicates that the AC inputs might be involved in some of the response patterns seen in these clusters. For example, in cluster 4, 72% of the neurons were from unlesioned mice, while neurons from unlesioned mice only accounted for 64% of the whole population. The response patterns of this cluster showed a distinct difference between hit and miss trials, displaying increased activity immediately following stimulus onset in hit but not miss trials. In cluster 6, neurons from lesioned mice accounted for 56% of the neurons in this cluster, while only 36% of the whole population was from lesioned mice. This cluster exhibited different but similar activity between hit and miss trials.

In summary, the unsupervised clustering algorithm revealed distinct clusters of CRIC neurons with different response dynamics during the sound-guided task. Neurons from both lesioned and unlesioned mice could be found in all of the clusters, while half of the clusters had more proportions of neurons from either lesioned or unlesioned mice than that of the whole population (**Figure 4.2**, **Figure A.3**). This implies that the AC could be involved in producing the specific response patterns seen in these clusters. The average responses of individual CRIC neurons were

heterogeneous across the population, exhibiting sound-evoked activity as well as different temporal profiles of sustained activity, likely reflecting behaviourally-relevant information.

5

Choice-related information in the CRIC network

Contents

5.1 CRIC network activity contained choice-related information regardless of AC inputs 54

5.2 Dynamic contributions of CRIC neurons to the decoding of choice-related information 57

The average responses of individual neurons exhibited a variety of activity patterns associated with stimulus and behavioural trial types. This raised further questions: How are these activity patterns read out collectively on a trial-by-trial basis? Does the CRIC network activity contain behaviourally-relevant information, such as whether the mouse successfully detected and reported a stimulus? Is this affected by the absence of AC inputs? To address these questions, logistic regression was trained on the activity of all the neurons identified in a given session to classify ("decode") hit versus miss trials on a trial-by-trial, frame-by-frame basis (see **Logistic regression** in 2.7). Logistic regression was used because it has the advantage over other classification algorithms in that it is generally more interpretable and takes into account all of the variables. The use of logistic regression also assumes that information could be read out linearly from the neural

activity. If the CRIC network activity contained information about whether correct choices were made in stimulus trials, the performance of the models would be significantly above chance level. Models were trained separately for each session, as different networks of neurons were identified in different sessions. The performance of "dummy models" was also evaluated to serve as the baseline model performance. Dummy models randomly classified trials while taking into account the probability of hit versus miss trials in a given session.

5.1 CRIC network activity contained choice-related information regardless of AC inputs

In both lesioned and unlesioned mice, the trained models performed significantly better than dummy models in classifying hit versus miss trials ($p < 0.05$, one-sided Wilcoxon signed-rank test or paired t-test with Bonferroni correction, **Figure 5.1b**). This suggested that the CRIC network activity contained information related to the behavioural choice of the mouse in stimulus trials, regardless of the presence of AC inputs. This information also lasted for at least 5 seconds after stimulus onset, which was longer than the dynamics of the calcium indicator. Interestingly, the trained models performed significantly better than dummy models even before the stimulus onset. This could indicate that the network activity before stimulus onset already contained some information about whether the upcoming stimuli would be detected and reported by the mouse.

Additionally, performance of the trained models in unlesioned mice was significantly better than those in lesioned mice around 1 - 4 seconds after stimulus onset (**Figure 5.1b**), indicating the CRIC network activity in unlesioned mice could be more accurately captured by the models in decoding choice-related information. However, this needs to be interpreted with caution, because the number of neurons identified in each session varied (**Figure 5.1a**), and significantly fewer neurons were identified in the fields of view of lesioned mice than those of unlesioned mice ($p < 0.001$, one-sided Mann-Whitney U test, median number of neurons for lesioned mice: 18, unlesioned: 38). This was likely due to experimental choices during

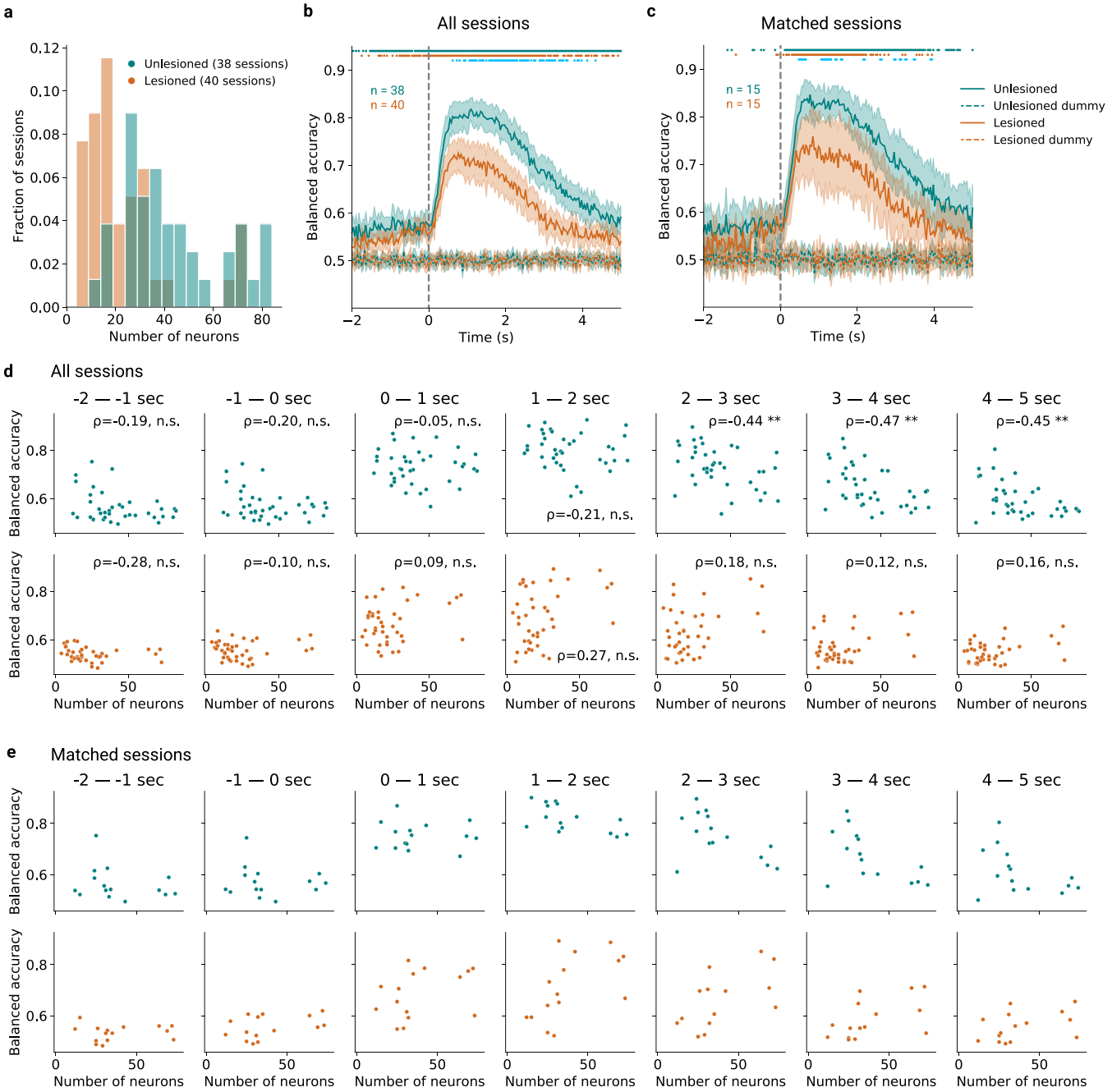

Figure 5.1: Choice-related activity was represented in the CRIC network, regardless of the presence of AC inputs. **(a)** Distribution of the number of neurons identified in each session. **(b)** Neural activity patterns contained information related to the behavioural choice of the mouse in stimulus trials. Data shown are the mean of the test results across sessions, shaded areas indicated 95% confidence intervals. Dots at the top indicated the timepoints where the model performance was significantly different between trained and dummy models for unlesioned mice (teal) or lesioned mice (orange), and between the trained models for unlesioned versus lesioned mice (blue) - see **Model comparisons** in 2.7. **(c)** Same as **(b)** but included only the sessions that had matched number of neurons (within ±5% difference) between lesioned and unlesioned mice (n = 15 sessions for each). **(d)** Correlation analysis between model performance and the number of neurons identified in each session. Between 2 - 5 sec following stimulus onset, the model performance was significantly negatively correlated with the number of neurons identified in unlesioned mice. Each data point represents the mean of the model performance within 1-sec windows in a given session. ρ: Spearman's correlation coefficient; **: $p < 0.01$. **(e)** Same as **(d)** but for matched sessions. Correlation analysis and testing were not performed as the number of samples was too small for estimation.

imaging experiments, such as the location and size of the field of view (see **Imaging Acquisition** in **Ch2.4**, **FigureA.4**). Since the number of neurons identified in sessions of lesioned mice was significantly lower than in those of unlesioned mice, it is possible that the measured neural activity contained less choice-related information simply because the number of neurons identified were lower. To assess if the decoding results were affected by the difference in the number of neurons, correlation analysis was conducted between the model performance and the number of neurons identified in each session. There were significant negative correlations between the number of neurons and the model performance 2 - 5 seconds following stimulus onset in unlesioned mice ($p < 0.01$, Spearman's correlation coefficient, **Figure 5.1d**). This suggests that had there been fewer neurons identified in the sessions of unlesioned mice, the difference in model performance found between lesioned and unlesioned mice would have been even greater.

To assess the model performance between lesioned and unlesioned mice without the confound of different numbers of neurons identified in the two groups, **Figure 5.1c** includes only the sessions matched for the number of neurons ("matched sessions" - within ±5% difference, see **Session sampling** in **Ch2.7**). The results followed a similar pattern as when including all the sessions - the CRIC network activity contained choice-related information on a trial-by-trial basis regardless of the presence of the AC inputs. The model performance of unlesioned mice was consistently better than that of lesioned mice across time, even though there were fewer timepoints that were significantly different (**Figure 5.1c**). The confidence intervals of the model performance in lesioned mice appeared to be larger, indicating the model performance was more variable across sessions in these animals. Indeed, the model performance in lesioned mice was more variable across sessions compared to that of unlesioned mice (**Figure 5.2**). Together, this implies that, without the inputs from the AC, the representation of choice-related information was more unreliable in the CRIC network, even though behaviourally there was no significant difference (**Figure 3.2**).

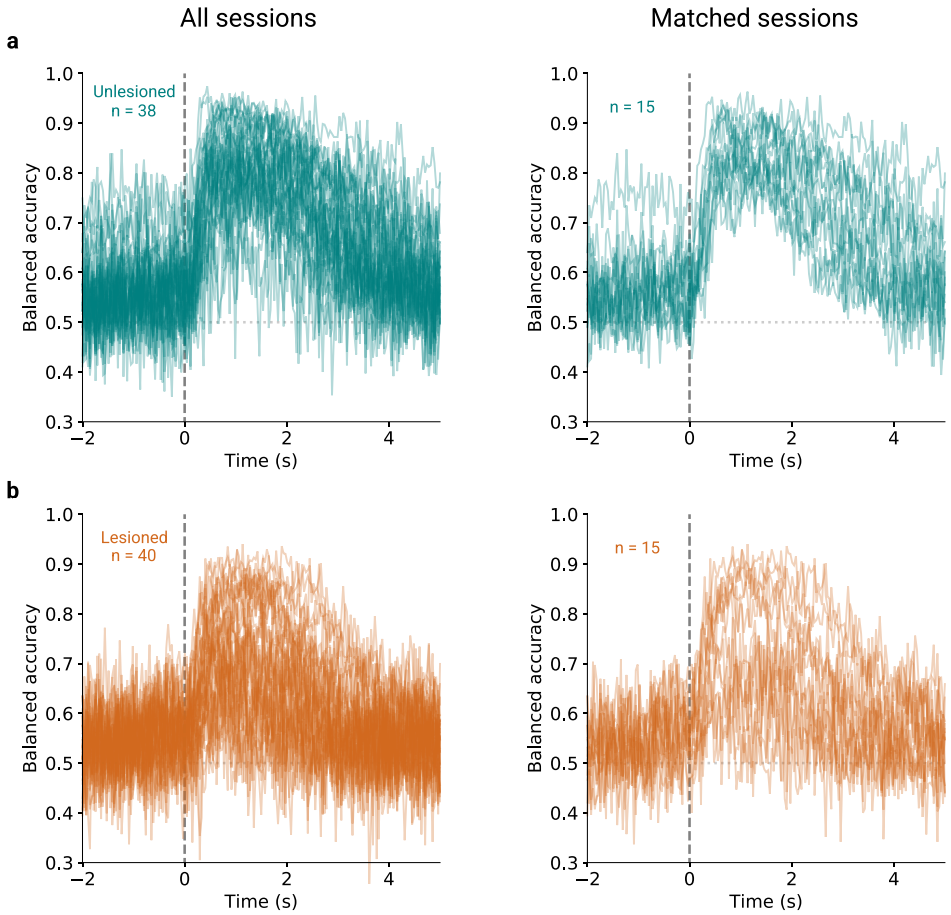

Figure 5.2: Decoding results for each individual session. Same as **Figure 5.1 (b-c)**, but displaying each session separately.

In summary, these results showed that there was behaviourally-relevant information in the CRIC network activity on a trial-by-trial basis, regardless of the presence of AC inputs. This information was more unreliable when the AC inputs were absent, suggesting that the AC might have a role in providing choice-related information to the CRIC network.

5.2 Dynamic contributions of CRIC neurons to the decoding of choice-related information

The results from the previous section raised further questions: How do neurons in the CRIC network contribute to the decoding of choice-related information? Was it the same neurons that contained choice-related information all the time, or different neurons at different time? How did this change when AC inputs were absent?

To gain insights into these questions, one could explore the coefficients of all the neurons in the logistic regression models. However, since the activity of neurons is correlated, exploring the model coefficients could give a misleading impression of how each neuron contributes to the models due to problems arise from collinearity (i.e. the situation where two or more predictor variables are closely related to one another) (James et al. 2021). To ensure the feature space of the models was uncorrelated so that the model coefficients could be more meaningfully explored, principal component analysis (PCA) was performed on the neurons axis across trials for each session at each timepoint. Using PC models offers the advantage that each PC is a linear combination of all the neurons and that PCs are not correlated by definition. The resulting principal components (PCs) could be interpreted as sub-populations of neurons that had similar activity patterns across trials at each timepoint. **Figure 5.3** shows the model performance with increasing number of PCs included as features of the models. Qualitatively, the model performance increased as a function of the number of PCs included in the models, and plateaued around 4-5 PCs for certain time windows following stimulus onset. Statistically, there was no significant difference between models trained with the activity of all neurons ("neuron models") and models trained with 2 or more PCs ("PC models"), apart from few timepoints at the end of the trials for lesioned mice in **Figure 5.3a** (top-right panel). Thus, statistically, the activity of a minimum of 2 sub-populations of neurons at each timepoint contained similar amount of choice-related information as the full neuron models. This allowed us to use the 2-PC models as an approximation of the neuron models, and to map the model coefficients of the PCs back to the neuron space to estimate how each neuron contributed to the decoding of choice-related information (see **Neuron contributions** in **Ch2.7**).

Figure 5.4 shows how each neuron contributed to the 2-PC models across time in each one of the matched sessions (see **Figure A.8** and **Figure A.9** for all of the sessions). Qualitatively, more neurons had higher contributions to the models after stimulus onset than before the stimulus, and their contributions started and peaked at variable timepoints and lasted for different amounts of time (**Figure 5.4**).

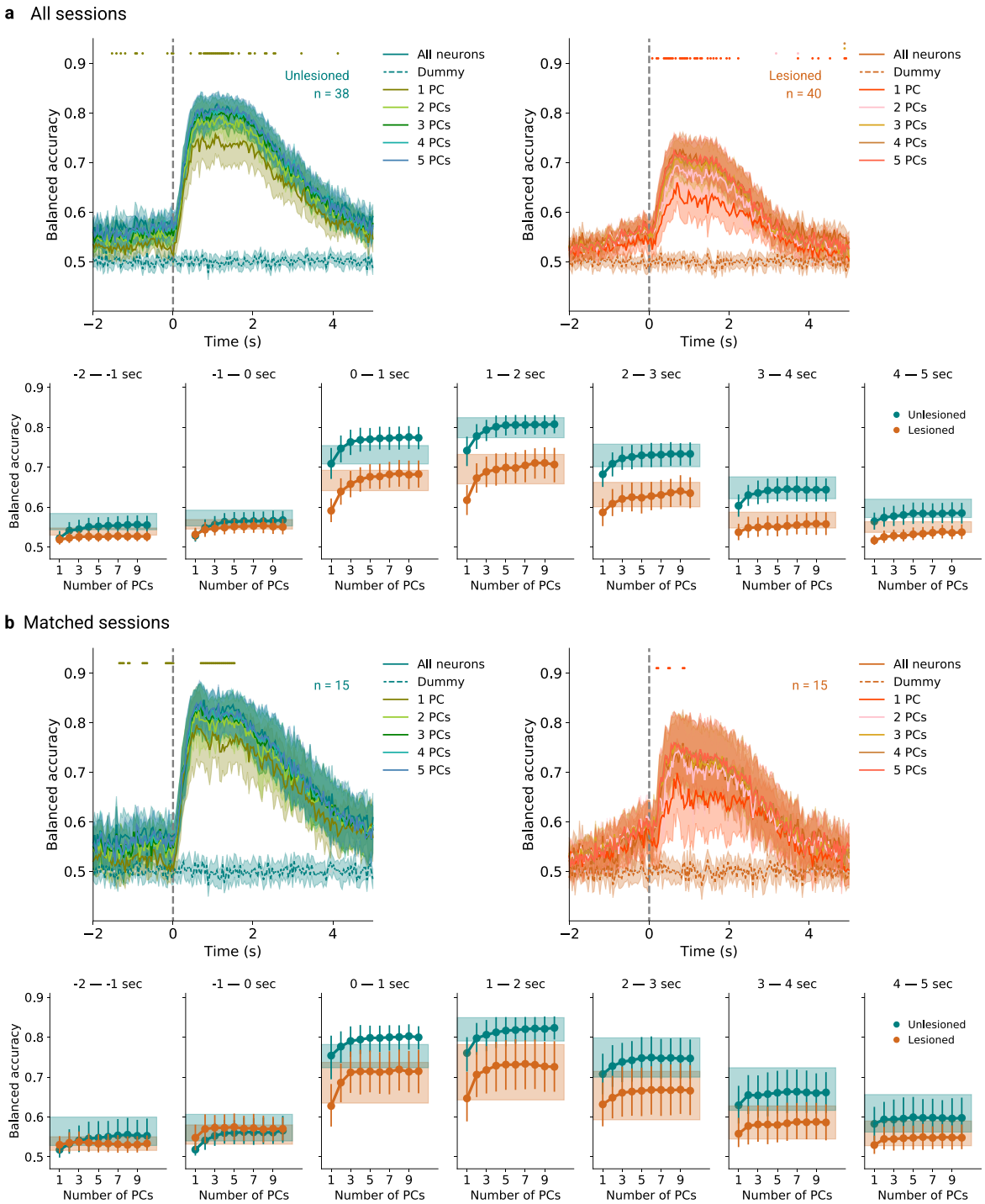

Figure 5.3: Activity of sub-populations of CRIC neurons containing choice-related information regardless of the presence of AC inputs. (a) Top: Decoding results with increasing number of PCs included in the models. Dots at the top are colour-coded by the number of PCs included, and indicate the timepoints where the performance of the neuron models and the PC models was significantly different ($p < 0.05$, one-sided Wilcoxon signed-rank test or paired t-test with Bonferroni correction). Bottom: The model performance for each 1-sec interval over the course of a trial. The mean model performance is shown within each 1-sec interval window of each session averaged across sessions. Error bars indicate 95% confidence intervals; shaded areas indicate the 95% confidence intervals of the neuron models. **(b)** Same as **(a)** but for the matched sessions (see **Session sampling** in 2.7).

On average, for both lesioned and unlesioned mice, around 90-100% of neurons contributed to the model performance with weights of 0 - 0.1 over the course of a trial (**Figure 5.5a,b**). After the stimulus onset, a small fraction of neurons that started to contribute with weights of 0.1 - 1.0 in unlesioned mice (**Figure 5.5a**) and weights of 0.1 - 0.7 in lesioned mice (**Figure 5.5b**). These results suggest that most of the neurons had similar, small, contributions (weights of 0 - 0.1) to the models before the stimulus onset, and after the stimulus onset, a small fraction of neurons became more important for decoding choice-related information. In unlesioned mice, some neurons were found to have a larger influence (higher weights) on the model performance than in lesioned mice, indicating that there were fewer neurons dominating the network for the decoding of choice-related information when AC inputs were removed.

To better understand whether it was always the same group of neurons that contributed to the decoding of choice-related information, or if the contributions were distributed across neurons, **Figure 5.5c-d** shows the fraction of the total number of time points for which each neuron contributed. The timepoints were only included if there was at least one neuron contributed to the models with the respective weights. The data in both lesioned and unlesioned mice shows that ~80% of the neurons that contributed with weights 0 - 0.1 contributed 90-100% of the time. For neurons that contributed with weights of 0.1 - 0.7 in unlesioned mice, the amount of time each neuron contributed was more varied, ranging between 0-100%; a similar pattern could be seen in lesioned mice for the neurons contributed with weights of 0.1 - 0.4. For neurons with weights of 0.9 - 1.0 in unlesioned mice and those with weights of 0.5 - 0.7 in lesioned mice, 100% of the neurons contributed to the models 100% of the time where there was at least one neuron contributing. This was simply because there were very few neurons with these higher weights (could be seen from **Figure 5.5a-b**, raw data not shown). Together, this suggests that neurons with weights of 0 - 0.1 contribute most of the time in both lesioned and unlesioned mice, while the contributions were distributed across neurons at



Figure 5.4: Patterns of neuron contributions to choice-related information. **(a)** Contributions of neurons to the performance of 2-PC models in matched sessions of unlesioned mice. Each heatmap represents a session, and the number at the top indicates the mouse's average behavioural performance (d') in that session for the stimuli included in the decoding models. Neurons were sorted by maximum contributions after stimulus onset. The order of the sessions displayed was sorted by the number of neurons identified in each session. Gray vertical dashed line indicates stimulus onset. A value of 0 indicates that either the model did not converge or the coefficient of the model was not significant (see **Neuron contributions** in 2.7). **(b)** Same as **(a)** but for sessions from lesioned mice.

different timepoints for those with higher weights of 0.1-0.7 in unlesioned mice and weights of 0.1 - 0.4 in lesioned mice.

In summary, statistically, the activity of a minimum of 2 sub-populations of neurons at each timepoint contained the same amount of choice-related information as the neuron models, which allowed us to use the 2-PC models as an estimate of the neuron models for assessing how each neuron contributed to the decoding of choice-related information. There were neurons in unlesioned mice that had a greater influence (higher weights) on the models than in lesioned mice, suggesting that there were fewer neurons dominating the network for the decoding of choice-related information when AC inputs were absent. On average, around 90-100% of neurons in both lesioned and unlesioned mice had a weight of 0 - 0.1 throughout the duration of the trial. After stimulus onset, a small fraction of neurons became more important for the decoding of the choice-related information, and their contributions were distributed across neurons and timepoints.

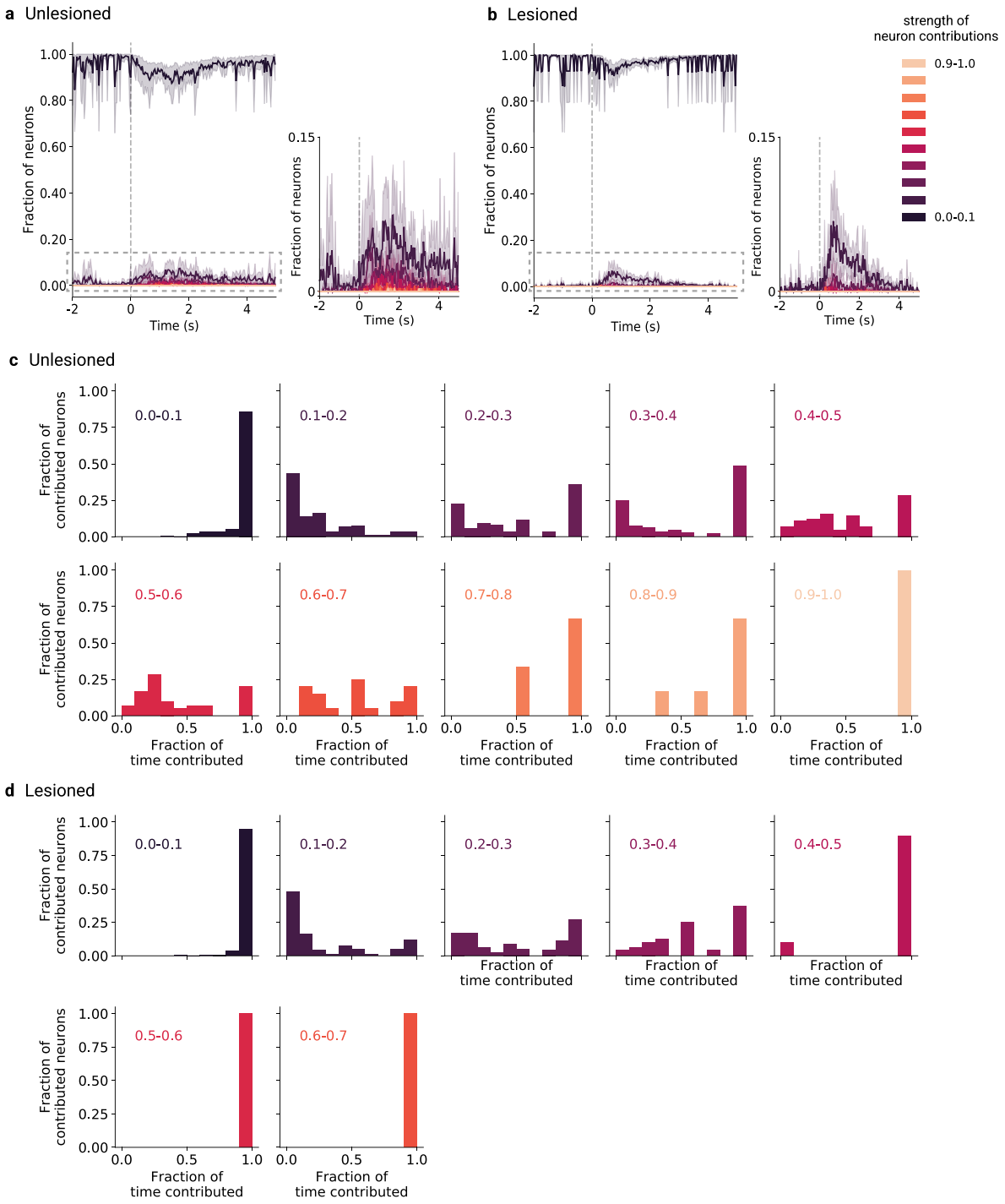

Figure 5.5: Dynamic contributions of neurons to the decoding of choice-related information. **(a)** Fraction of neurons that contributed to the 2-PC decoding models over the course of a trial in matched sessions of unlesioned mice. Data were averaged across sessions, shaded areas indicate 95% confidence intervals. The inset shows a magnified version of the area marked by the dashed line, including only neurons with weights of more than 0.1. **(b)** Same as **(a)** but for lesioned mice. **(c)** Fraction of time neurons contributed in matched sessions of unlesioned mice. Data were averaged across sessions. For each weight, only neurons that contributed with this strength and only the time bins where there was at least one contributing neuron in a given session were included. **(d)** Same as **(c)** but for lesioned mice.

6 Discussion

Contents

6.1 Involvement of the AC in sound detection 66
6.2 Manipulation of the CC pathway 67
6.3 Individual neuronal response profiles 68
6.4 Choice-related information in the CRIC network . . . 69
6.5 Neuron contributions to the decoding of choice-related information 70
6.6 Pre-stimulus activity 71
6.7 Future work 72

Our perception is shaped by both external inputs and internal information, such as our memories and past experiences. This suggests that sensory processing involves the integration of both bottom-up sensory inputs as well as top-down feedback connections from higher brain areas. While much research has focused on studying sensory processing along the ascending pathways, how descending projections contribute to earlier stages of sensory processing remains relatively unclear. Understanding the role of descending connections is important as they are essential elements of the neural computation for sensory processing and behaviour.

In this thesis, I studied one of the major descending circuits in the central auditory system, the cortico-collicular (CC) pathway. I developed an automatic behavioural training paradigm and data management systems for efficient and reproducible

data collection and processing (**Figure 2.1, 3.2**). Behavioural experiments showed that mice were able to learn and perform a sound detection task regardless of the presence of the AC, and there was no significant difference from control animals in their ability to learn across days or to detect sound stimuli of different amplitudes (**Figure 3.2**). By recording the activity of cortico-recipient inferior colliculus (CRIC) neurons during behaviour, I found that the average population response across all neurons exhibited different response profiles following stimulus onset for reported vs non-reported stimuli (**Figure 4.1**). Furthermore, individual CRIC neurons exhibited heterogeneous averaged response profiles with or without AC inputs, including evoked activity immediately following sound onset and different temporal profiles of sustained activity (**Figure 4.2**), likely reflecting behaviourally-relevant information. Some patterns of activity were more prominent in either lesioned or unlesioned mice (**Figure 4.2**), implicating the involvement of the AC in those response dynamics. Population decoding revealed that the CRIC network activity contained trial-by-trial behaviourally-relevant information (**Figure 5.1**), which was more unreliable when the AC input was removed (**Figure 5.2**). In both lesioned and unlesioned mice, a small fraction of neurons became more important for the decoding of choice-related information after stimulus onset, and their contributions were distributed across neurons and timepoints (**Figure 5.4, 5.5**). There were neurons in unlesioned mice that had higher influences on the models than in lesioned mice, implying that there were fewer neurons dominating the network for the decoding of choice-related information when the AC input was absent (**Figure 5.4, 5.5**).

Overall, this work offers novel insights into the neural and behavioural function of the auditory CC pathway. The hope is that this will contribute to our overall understanding of the role of feedback connections in sensory processing and behaviour. This section will further discuss the interpretations and limitations of the findings, as well as future research directions arising from the results of this work.

6.1 Involvement of the AC in sound detection

Consistent with previous studies, we found that mice with bilateral AC lesions were able to learn and perform a sound detection task as well as mice with an intact cortex[1](**Chapter 3.1**), even though some of the previous studies using pharmacological inactivation or lesions have shown that the primary AC is required to execute simple auditory tasks after animals were trained (Heffner and Heffner 1990, Talwar et al. 2001, Heffner and Heffner 2003, Li et al. 2017). Similar results were found recently in the somatosensory system, where permanent lesions of the somatosensory cortex before learning did not affect the learning of a tactile detection task, while lesions after learning initially impaired task performance but this recovered by the subsequent session (Hong et al. 2018). In the motor system, the motor cortex was shown to be required for learning but not executing temporally precise motor sequences (Kawai et al. 2015). One possibility is that if sensory cortices were absent before learning, subcortical areas, such as the midbrain or the thalamus, could take over some of the sensory processing that is otherwise primarily performed by the cortex (Talwar et al. 2001). This would be consistent with the results that inactivation of the AC impaired sound detection after learning (Li et al. 2017), while lesions before learning did not (**Figure 3.2**).

Future research could track the responses of subcortical areas (and corticollicular neurons or their axons) during learning and behaviour, with some mice lesioned before learning and others after learning. This could provide insights into whether a recovery of behavioural performance could be seen as in Hong et al. 2018, and reveal potential differences in subcortical processing between the two scenarios. For instance, if certain patterns of activity only exist during or after learning when the AC was absent, it could indicate that these activity patterns were important for the

[1]It is worth bearing in mind that there were some differences in the behavioural training conducted by different experimenters as described in Chapter 2.3.1, which might influence the learning and behaviour. For example, the reaction time of the mice might have been different, but since the response window was varied in some mice in this present study, comparing the reaction time across mice could be misleading.

processing that compensates the absence of the AC. It would then be interesting to see if these patterns emerge in mice that have lesions after learning. Further analysis could also reveal if these potential changes correlate with the extent of lesions.

6.2 Manipulation of the CC pathway

Lesions ensures a more complete inactivation of the AC, however, AC lesions not only removed the CC connections, but also the projections from the AC to other cortical and subcortical areas, which may or may not cause unspecific effect on the the observed responses of the CRIC neurons. To allow more precise manipulation of the CC pathway, 7 different optogenetics strategies were attempted for developing the techniques to silence the AC axons in the IC while imaging IC neurons. Among them, AAV8-Flex-Jaws could not be expressed correctly in the AC, and 2 of the transgenic lines exhibited too sparse expression of either GCaMP in the IC neurons (CaMKIIα-Cre-GCaMP6f mice) or Cre in the AC neurons (CaMKIIα-Cre-3487 mice), which was not ideal as it means few IC neurons could be imaged or few AC axons would be silenced. When expressing AAV1-hSyn-Cre and AAV1-flex-jaws in the AC and optogenetically stimulate the AC axons in the IC, a small suppression was observed in the CRIC responses, unexpectedly, no AC neurons or axons were identifiable when histological images were examined. However, when expressing AAV1-flex-jaws in Rbp4-Cre mice (instead of using viral delivery of Cre), AC neurons and axons were clearly labelled with AAV1-flex-jaws, even though laser stimulation of the AC axons showed no effect on the responses of tuned IC neurons. There could be several possible reasons, for example, the laser stimulation was not able to silence large enough population of axons or could not sufficiently activate the opsins, even though we have successfully activated the AC axons in the IC with Chrimson using the same set up and procedure. It is also likely that some of the IC neurons imaged do not receive AC inputs, hence they were not directly affected by the inactivation of AC axons. In addition, only neurons that were tuned were included in the analysis, while the laser stimulation may have an effect on other neurons. Further analysis could include all neurons and re-examine the results.

Another possible scenario could be that optogenetic silencing of the CC pathway had no effect on the IC responses during passive listening conditions (Blackwell et al. 2019). This study optogenetically inhibited the auditory CC neurons and found no effect on IC responses. To test if this might be the case, the Rbp4-Cre mice injected with AAV1-flex-jaws and AAV1-Syn-GCaMP6f were trained on the sound detection task while stimulating the axons. Due to the low number of mice and limited time, the effect of silencing AC axons on IC neurons remain unclear. Further experiments and analysis would be needed, potentially include further optimisation of the viral concentration and the opsins used.

6.3 Individual neuronal response profiles

We observed sound-evoked activity in stimulus trials in the average CRIC population response across all recorded neurons, and sustained activity could only be seen in hit but not miss trials in mice with or without the AC (**Figure 4.1**). This indicates that the average CRIC population response might contain behaviourally-relevant information irrespective of AC input. Further investigation into the response dynamics of individual CRIC neurons revealed that they display heterogeneous responses, forming 10 clusters of activity patterns (**Figure 4.2**). Half of the clusters included a greater proportion of neurons from either lesioned or unlesioned mice than that of the whole population, implying that the AC could be involved in influencing the specific response patterns seen in these clusters.

The goal of clustering analysis is to find an informative way to visualize the data and to uncover subgroups of neurons with distinct properties (James et al. 2021). However, a caveat of clustering analysis in general is that it could generate different results across different algorithms as there are many different ways to cluster data, and that some cluster analyses will generate slightly different results because of different initial starting points of the algorithm (James et al. 2021). Spectral clustering was used because it has been argued that this produces stable results in high-dimensional neural data (Hirokawa et al. 2019), and that the optimal Silhouette Score for this approach was better than that of other clustering methods,

such as k-means or hierarchical clustering, for similarly constructed high-dimensional neural data (Namboodiri et al. 2019). The results shown in **Chapter 4.2** were optimised through a grid search over the parameter space, and different initial starting points produced similar results. The clusters had clear differences in their response patterns and offer insights into the heterogeneity of the averaged responses of individual neurons in both lesioned and unlesioned mice.

The aim of the clustering analysis used here was to identify distinct response dynamics that might be affected by the removal of CC inputs, and which could therefore implicate the involvement of the AC in those activity patterns. Further analysis, such as regression analysis, could be performed to examine which task variables were encoded in the activity of neurons in each cluster. It would also be interesting to investigate how these clusters evolve during learning, and to examine which of the activity patterns already exist before learning and which ones only emerged afterwards.

6.4 Choice-related information in the CRIC network

While the clustering analysis highlights the heterogeneity of the average responses of individual neurons in an unsupervised way, classification algorithms (e.g. logistic regression) are supervised methods for testing whether the neural activity could be read out collectively and contains choice-related information on a trial-by-trial basis. It is important to bear in mind that decoding models using classification techniques are a way of estimating if specific information exists in the patterns of neural activity, and not necessarily how the brain carries out these computations.

Choice-related information includes signals associated with the animals' choice, such as decisions, movements, and rewards. The presence of such information in the CRIC network could help generate more robust representations of sensory stimuli that are behaviourally-relevant (Souffi et al. 2021). The decoding analysis revealed that choice-related information could be decoded from the trial-by-trial CRIC network activity regardless of the presence of the AC (**Figure 5.1**), and that

this information was more unreliable when AC inputs were absent (**Figure 5.2**). Interesting activity patterns from the clustering analysis could potentially help explain this finding, especially in clusters 4 and 6 where the proportion of neurons from lesioned and unlesioned mice deviated the most from the overall population (**Figure 4.2**). Neurons in cluster 4 exhibited a clear distinction between hit and miss trials, and the proportion of neurons from unlesioned mice in this cluster was significantly greater than that in the overall population. Cluster 6 showed similar activity in hit and miss trials following stimulus onset (indicating that it could be harder to classify hit versus miss trials based on the neural activity), and neurons from lesioned mice accounted for a significantly greater proportion in this cluster than in the overall population. Further analysis may show whether the proportion of neurons from cluster 4 and 6 (or any other cluster) in each session is correlated with the performance of the decoding models.

Together, these results suggest that while choice-related information in the activity of these IC neurons was present irrespective of the presence of CC inputs, the AC may play a role in providing more reliable choice-related information to the network of CRIC neurons. Further analysis could reveal whether the decoding performance correlates with the extent of lesions in each mice. Choice-related information could be associated with various signals when animals made the choice to report the detected stimuli, including the behavioural decision, associated reward, or motor and somatosensory signals (Metzger et al. 2006, Chen and Song 2019, Yang et al. 2020, Lohse et al. 2021). These signals could reach the IC via direct CC pathway or other indirect pathways, such as through the somatosensory, motor, and frontal areas (Gruters and Groh 2012, Olthof et al. 2019, Souffi et al. 2021), which would be an interesting avenue of research for future studies to explore.

6.5 Neuron contributions to the decoding of choice-related information

Further investigation of the weights of each neuron in the decoding models revealed how individual neurons in the CRIC network contributed to the decoding of choice-

related information. While interpreting these weights, one should keep in mind that it is based on the decoding models that were built, and not necessarily how these neural signals were read out in the brain. Nevertheless, exploring the weights of the models is one step closer to gaining insights into how these neurons might contribute to the choice-related information in the CRIC network.

Analysis of the weights showed that a small fraction of neurons became more important for decoding choice-related information after stimulus onset, and their contributions were distributed across time and neurons (**Figure 5.4, 5.5**). The results also indicate that there were fewer neurons dominating the network for the decoding when AC inputs were removed (**Figure 5.5**). It would be interesting to further explore the physiological and anatomical properties of the neurons with high weights (i.e. influencing the decision of the models more), and if they were from specific clusters at specific times in a trial.

The contributions of each neuron to the models were estimated using PC models for reasons discussed in **Chapter 5.2**. 2-PC models were used since they contained the minimum number of PCs where the model performance was not significantly different from that of full neuron models. This is also based on the assumption that the directions in which the neural activity varies the most at each timepoint in a high-dimensional space are most associated with the mouse's choice in a stimulus trial (i.e. hit vs miss). Further analysis could include adding more PCs with appropriate regularisation and comparing this to the results reported in the thesis.

6.6 Pre-stimulus activity

We observed pre-stimulus activity in the CRIC neurons that differed between hit and miss trials (**Figure 4.2, 5.1**). This could be seen from the elevated averaged responses of individual neurons before stimulus onset in either hit or miss trials (cluster 7 and 9, **Figure 4.2**), as well as the above-chance-level decoding model performance before stimulus onset (**Figure 5.1**). This is intriguing because there were no task-related cues before the stimulus onset and the inter-trial interval of the behavioural task was random, yet these signals correlated with the outcome

of an upcoming trial (i.e. whether an upcoming stimulus would be reported or not). This activity is not associated with licking since hit trials were excluded from analysis if any licks occurred between -0.5 to +0.12 seconds relative to stimulus onset (See **Chapter 2.3.3**).

One possibility is that the activity before stimulus onset relates to the state of the network and the behavioural state of the animals, which could affect the detection of an upcoming stimulus. Factors such as attention, arousal, and the motivational state of the animals could all be affecting sensory detection on a trial-by-trial basis (Lee and Dan 2012, McGinley et al. 2015). A recent study showed that the variance of the population activity before stimulus presentation was predictive of trial outcome, and the population variance was correlated with task variables that implicate the motivational state of animals (Rowland et al. 2021). Similar analysis could be conducted on our data set, as well as to explore whether arousal state as assessed by pupil diameter is associated with the observed pre-stimulus activity. The activity of L4 and L5 AC neurons has been shown to correlate with the arousal state of the animals (McGinley et al. 2015), while the IC also exhibits increased activity during behaviour compared to passive listening (Ryan and Miller 1977, Ryan et al. 1984) and receives inputs from the locus coeruelus (LC) (Hurley 2018), which has been implicated in arousal (Aston-Jones and Cohen 2005). Thus, it would be interesting to explore whether the activity of the CRIC neurons was correlated with the animal's arousal level before stimulus presentation, and to what extent this depends on the input from the AC.

6.7 Future work

Overall, this work offers novel insights into the neural and behavioural function of the CRIC neurons with or without AC inputs, at both individual neuron level and network level. As outlined above, further work is required to fully understand the function of the auditory CC pathway. For example, it would be essential to more selectively manipulate the CC pathway and assess the behavioural and neural consequences of this in challenging behavioural tasks, as the CC pathway could be

more engaged in such scenarios (Bajo et al. 2010, Souffi et al. 2021). Longitudinal tracking of the same neurons would also reveal how the clusters and choice-related information evolve over the course of learning, and temporally precise inactivation techniques could uncover the role of the CC pathway at different stages of behaviour or task events. Further questions remain; for instance, how does the top-down AC input to the CRIC neurons influence the computations within the IC and along the ascending and descending pathways? How do other neuromodulatory and non-auditory inputs interface with this? Exploring these questions would allow us to get a better understanding of the neural and behavioural function of the auditory CC pathway, which will in turn improve our understanding of the diverse roles of descending connections in sensory processing and behaviour. The approaches developed in this thesis pave the way for investigating these questions specifically in the neurons that are targeted by descending cortical inputs.

Appendices

A

Supplementary figures

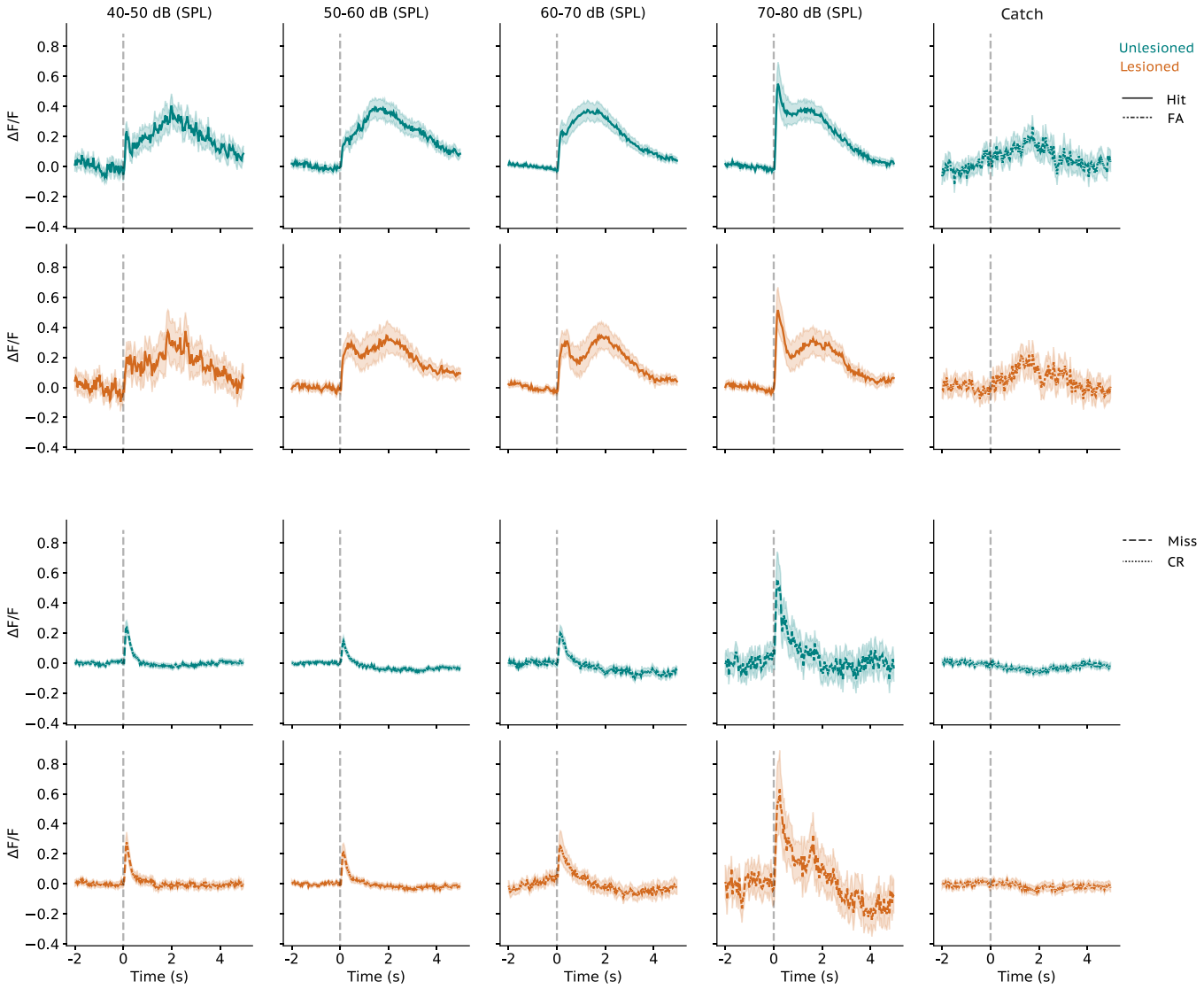

Figure A.1: Average population response profiles for each trial type. Same as **Figure 4.1d** but displaying the responses for each trial type separately.

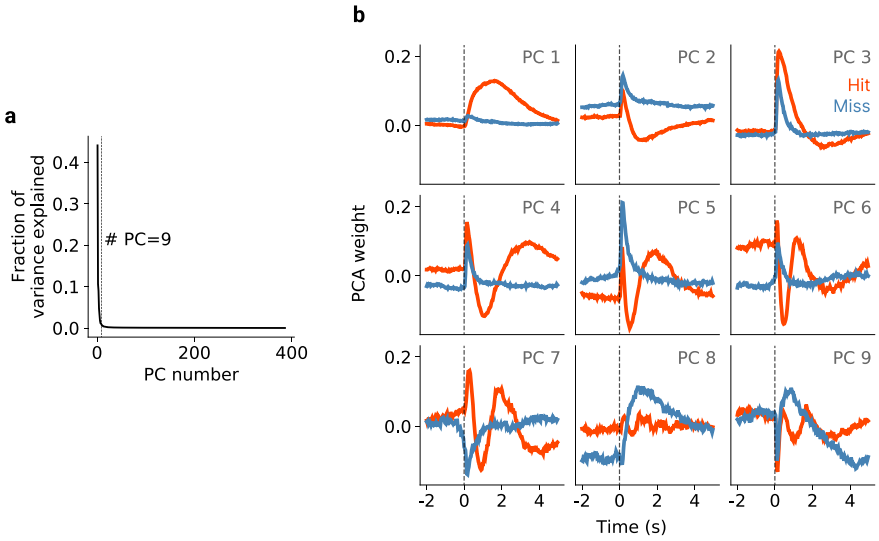

Figure A.2: Principal components as inputs to the clustering algorithm. (a) Scree plot showing the fraction of variance explained for each principal component (PC). The vertical dashed line indicates the "elbow" point, which is the point that exhibits a sharp decrease in the slope of the curve from one PC to another, followed by a more gradual decrease in slope. The standard method for choosing the number of PCs to keep is to find the last value of the PC before the slope of the plot went flat, which corresponds to PC 9 here. **(b)** The activity of the first 9 PCs in hit vs miss trials.

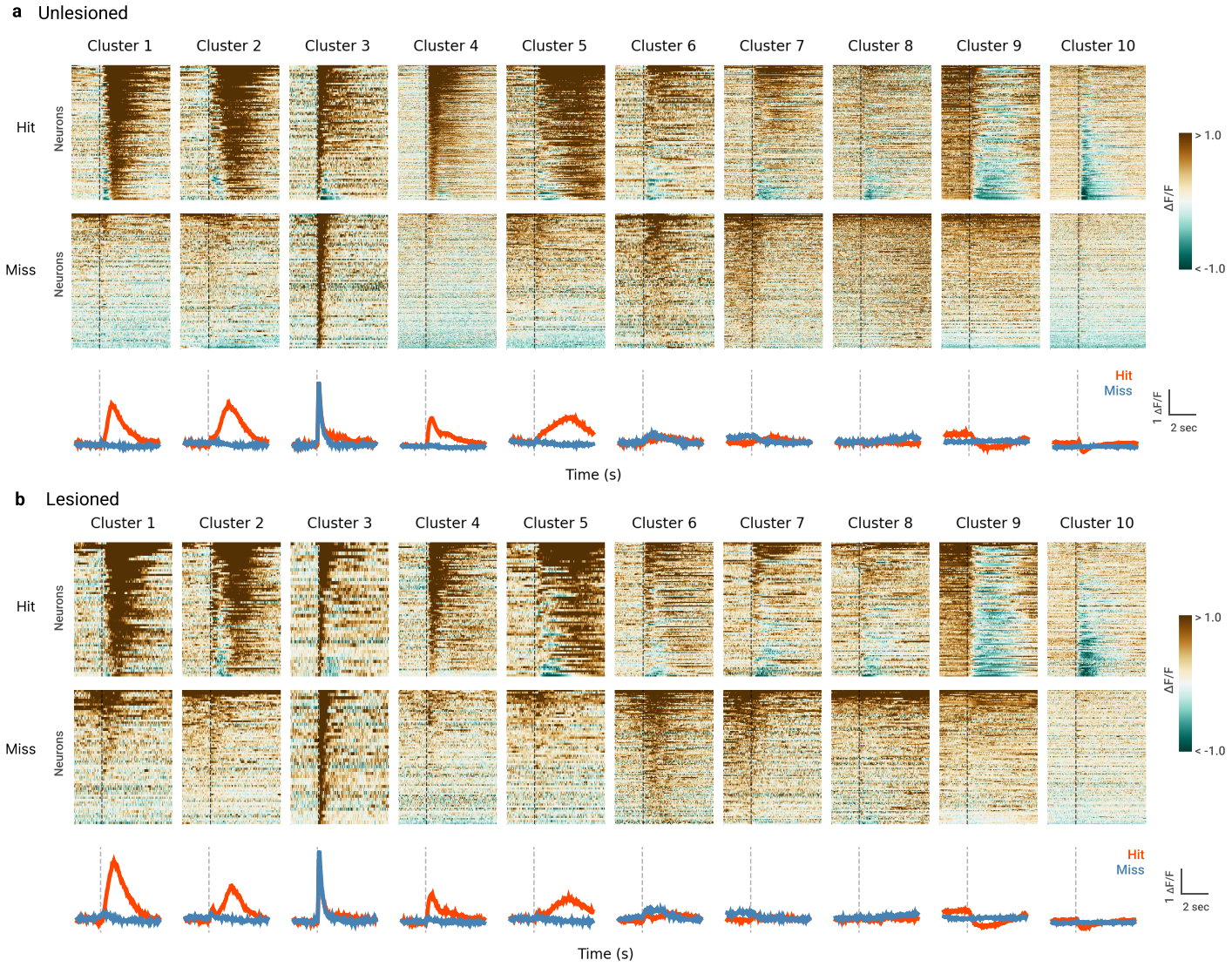

Figure A.3: Response profiles of neurons from unlesioned vs lesioned mice for each cluster. Same as **Figure 4.2b,c** but displaying neurons from unlesioned **(a)** and lesioned **(b)** mice separately.

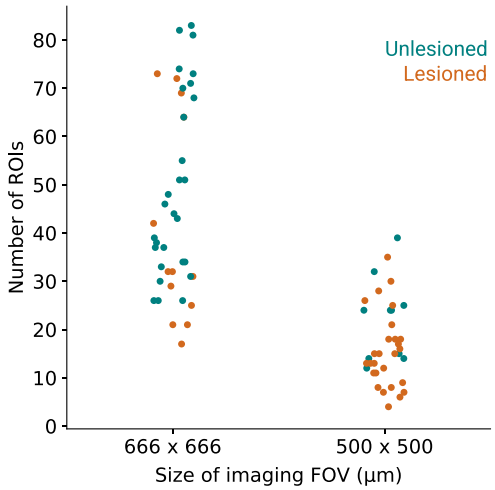

Figure A.4: Number of neurons identified per session. Each data point represents the number of neurons identified in a given imaging session used in decoding analysis.

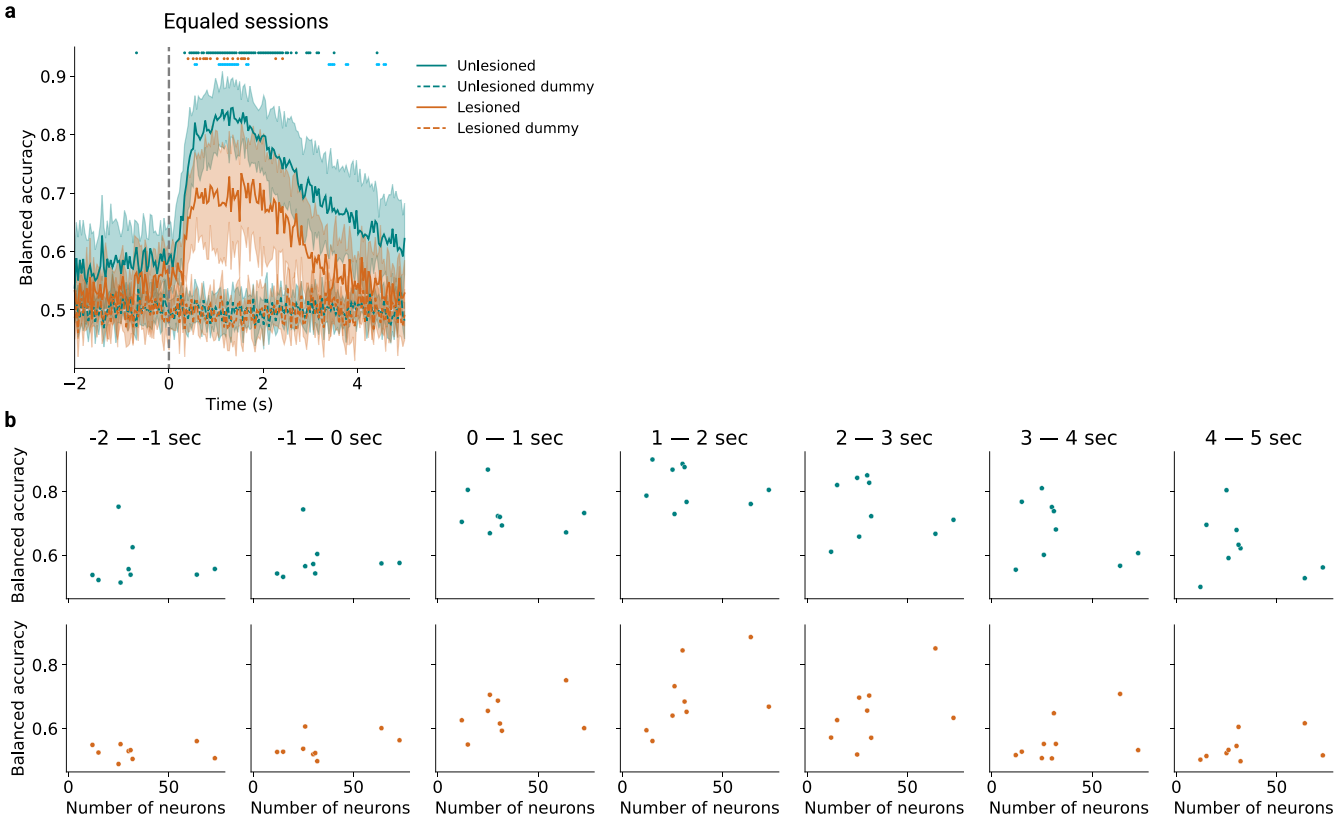

Figure A.5: Decoding results for sessions with equal number of neurons. Same as **Figure 5.1 (c,e)** but included only the sessions that had equal number of neurons between lesioned and unlesioned mice. Specifically, equal number of sessions were pooled from lesioned and unlesioned mice, where the number of neurons identified in these sessions were the same between each pair of sessions.

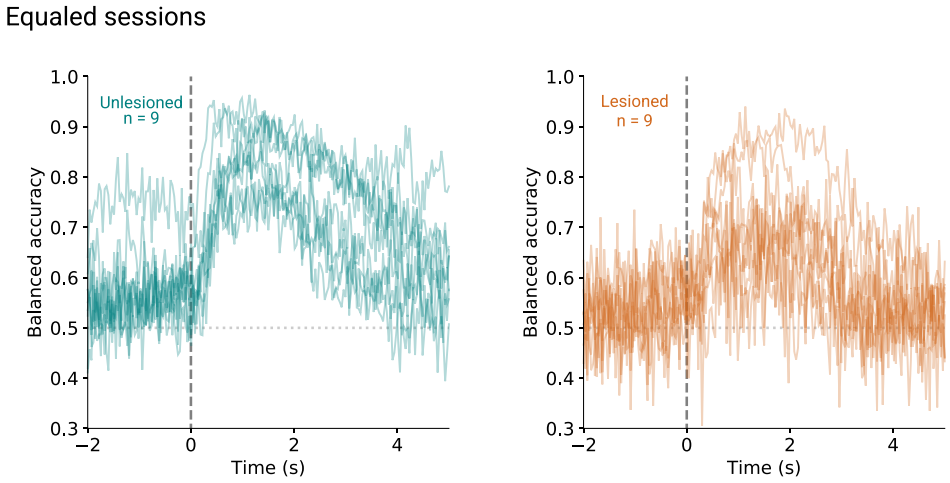

Figure A.6: Decoding results for each individual session included in equaled sessions. Same as **Figure A.5 (a)**, but displaying each session separately.

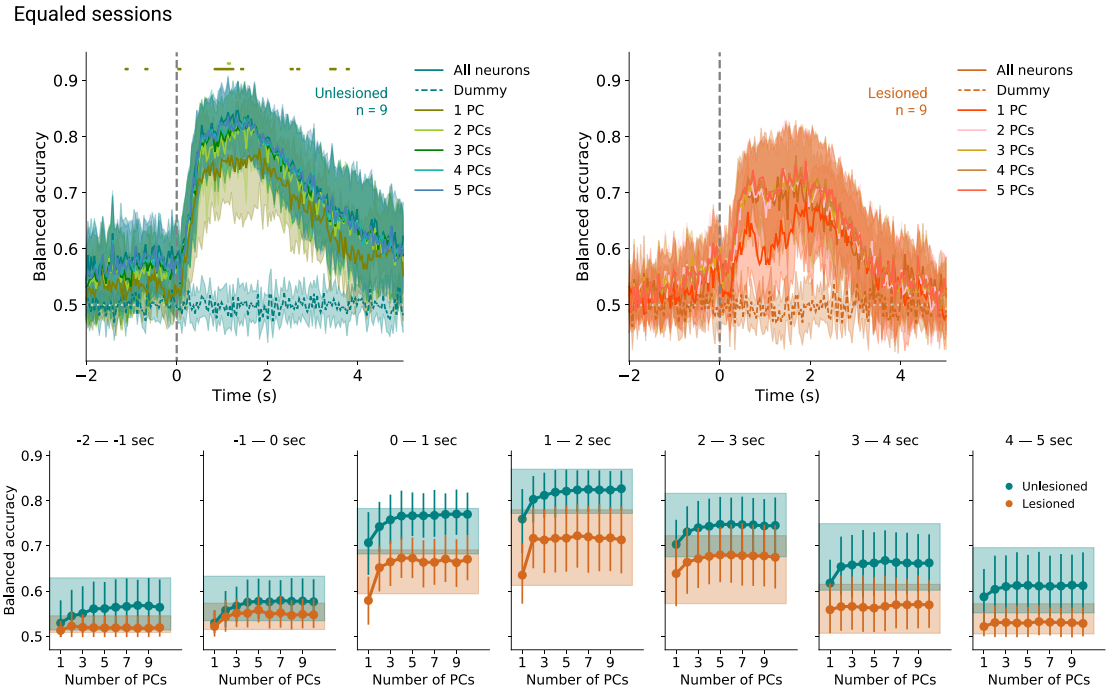

Figure A.7: Decoding results with increasing number of PCs included in the models for equaled sessions. Same as **Figure 5.3** but for equaled sessions.

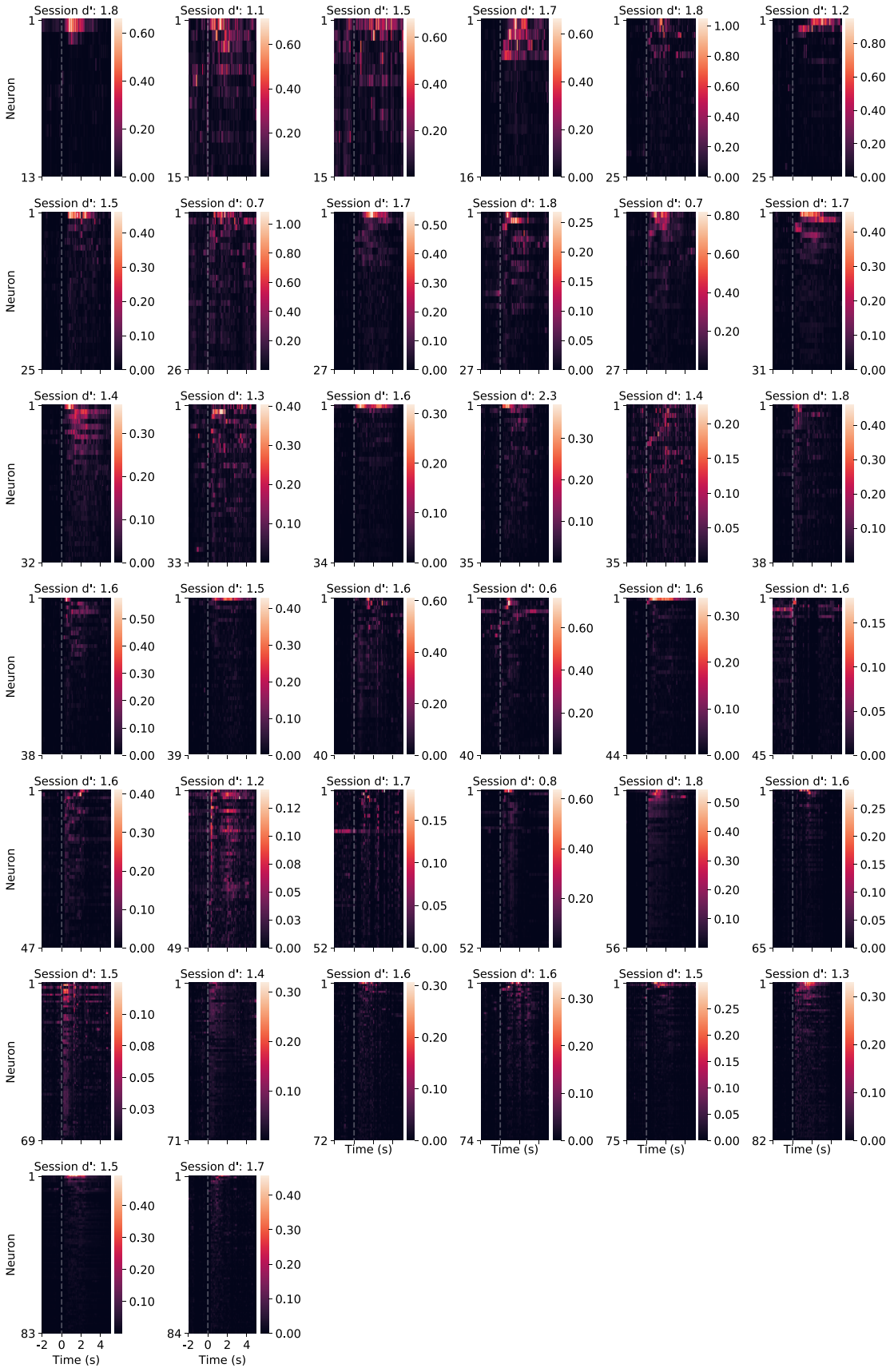

Figure A.8: Contributions of neurons to choice-related information for all sessions from unlesioned mice. Same as **Figure 5.4a** but included all sessions.



Figure A.9: Contributions of neurons to choice-related information for all sessions from lesioned mice. Same as **Figure 5.4b** but included all sessions.

References

Adams, Joe C. (1980). "Crossed and descending projections to the inferior colliculus". In: *Neuroscience Letters* 19, pp. 1–5.

Aitkin, Lindsay M., C. E. Kenyon, and Paolo G. Daniel Philpott (1981). "The representation of the auditory and somatosensory systems in the external nucleus of the cat inferior colliculus". In: *Journal of Comparative Neurology* 196.

Aitkin, Lindsay M. et al. (1978). "External nucleus of inferior colliculus: auditory and spinal somatosensory afferents and their interactions." In: *Journal of neurophysiology* 41 4, pp. 837–47.

Asokan, Meenakshi M. et al. (2018). "Sensory overamplification in layer 5 auditory corticofugal projection neurons following cochlear nerve synaptic damage". In: *Nature Communications* 9.

Aston-Jones, Gary and Jonathan D. Cohen (2005). "An integrative theory of locus coeruleus-norepinephrine function: adaptive gain and optimal performance." In: *Annual review of neuroscience* 28, pp. 403–50.

Bajo, Victoria M. and Andrew J. King (2013). "Cortical modulation of auditory processing in the midbrain". In: *Frontiers in Neural Circuits* 6.

Bajo, Victoria M. and David R. Moore (2005). "Descending projections from the auditory cortex to the inferior colliculus in the gerbil, Meriones unguiculatus". In: *Journal of Comparative Neurology* 486.

Bajo, Victoria M. et al. (2007). "The ferret auditory cortex: descending projections to the inferior colliculus." In: *Cerebral cortex* 17 2, pp. 475–91.

Bajo, Victoria M. et al. (2010). "The descending corticocollicular pathway mediates learning-induced auditory plasticity". In: *Nature Neuroscience* 13, pp. 253–260.

Barnstedt, Oliver et al. (2015). "Functional Microarchitecture of the Mouse Dorsal Inferior Colliculus Revealed through In Vivo Two-Photon Calcium Imaging". In: *The Journal of Neuroscience* 35, pp. 10927–10939.

Blackwell, Jennifer M. et al. (2019). "Auditory cortex shapes sound responses in the inferior colliculus". In: *eLife* 9.

Brodersen, Kay Henning et al. (2010). "The Balanced Accuracy and Its Posterior Distribution". In: *2010 20th International Conference on Pattern Recognition*, pp. 3121–3124.

Brophy, Alfred L. (1986). "Alternatives to a table of criterion values in signal detection theory". In: *Behavior Research Methods, Instruments, & Computers* 18, pp. 285–286.

Bulkin, David A. and Jennifer M. Groh (2012). "Distribution of visual and saccade related information in the monkey inferior colliculus". In: *Frontiers in Neural Circuits* 6.

Calford, Michael B. and Lindsay M. Aitkin (1983). "Ascending projections to the medial geniculate body of the cat: evidence for multiple, parallel auditory pathways through thalamus". In: *The Journal of neuroscience : the official journal of the Society for Neuroscience.*

Casseday, John H., Thane Fremouw, and Ellen Covey (2002). *The Inferior Colliculus: A Hub for the Central Auditory System.*

Ceballo, Sebastián et al. (2019). "Targeted Cortical Manipulation of Auditory Perception". In: *Neuron* 104, 1168–1179.e5.

Chaigneau, Emmanuelle et al. (2011). "Impact of wavefront distortion and scattering on 2-photon microscopy in mammalian brain tissue". In: *Optics Express* 19, pp. 22755–22774.

Chakravarthy, Sridhara et al. (2006). "Postsynaptic TrkB signaling has distinct roles in spine maintenance in adult visual cortex and hippocampus." In: *Proceedings of the National Academy of Sciences of the United States of America* 103 4, pp. 1071–6.

Chen, Chenggang and Sen Song (2019). "Differential cell-type dependent brain state modulations of sensory representations in the non-lemniscal mouse inferior colliculus". In: *Communications Biology* 2.

Chen, Chenggang et al. (2018). "Neuronal Organization in the Inferior Colliculus Revisited with Cell-Type-Dependent Monosynaptic Tracing". In: *The Journal of Neuroscience* 38, pp. 3318–3332.

Chen, Tsai-Wen et al. (2013). "Ultra-sensitive fluorescent proteins for imaging neuronal activity". In: *Nature* 499, pp. 295–300.

Codd, E. F. (1970). "A relational model of data for large shared data banks". In: *M.D. computing : computers in medical practice* 15 3, pp. 162–6.

Druga, R, Josef Syka, and Grazyna Rajkowska (1997). "Projections of auditory cortex onto the inferior colliculus in the rat." In: *Physiological research* 46 3, pp. 215–22.

Gruters, Kurtis G. and Jennifer M. Groh (2012). "Sounds and beyond: multisensory and other non-auditory signals in the inferior colliculus". In: *Frontiers in Neural Circuits* 6.

Hackett, Troy A. et al. (2011). "Linking Topography to Tonotopy in the Mouse Auditory Thalamocortical Circuit". In: *The Journal of Neuroscience* 31, pp. 2983–2995.

Harris, Kenneth D. et al. (Aug. 26, 2016). "Improving data quality in neuronal population recordings". In: *Nature Neuroscience* 19.9, pp. 1165–1174.

Hautus, Michael J. (1995). "Corrections for extreme proportions and their biasing effects on estimated values ofd". In: *Behavior Research Methods, Instruments, & Computers* 27, pp. 46–51.

Haxby, James V. et al. (2001). "Distributed and Overlapping Representations of Faces and Objects in Ventral Temporal Cortex". In: *Science* 293, pp. 2425–2430.

Heffner, Henry E and Rickye S. Heffner (1990). "Effect of bilateral auditory cortex lesions on absolute thresholds in Japanese macaques." In: *Journal of neurophysiology* 64 1, pp. 191–205.

— (2003). "Audition". In: *Handbook of Research Methods in Experimental Psychology*, pp. 413–440.

Helmchen, Fritjof and Winfried Denk (2005). "Deep tissue two-photon microscopy". In: *Nature Methods* 2, pp. 932–940.

Herbert, Horst, Andreas Aschoff, and Joachim Ostwald (1991). "Topography of projections from the auditory cortex to the inferior colliculus in the rat". In: *Journal of Comparative Neurology* 304.

Hirokawa, Junya et al. (2019). "Frontal cortex neuron types categorically encode single decision variables". In: *Nature*, pp. 1–6.

Hong, Y. Kate et al. (2018). "Sensation Movement and Learning in the Absence of Barrel Cortex". In: *Nature* 561, pp. 542–546.

Huang, Camillan and Jeffery A. Winer (2000). "Auditory thalamocortical projections in the cat: Laminar and areal patterns of input". In: *Journal of Comparative Neurology* 427.

Hubel, David H. and Torsten N. Wiesel (1962). "Receptive fields, binocular interaction and functional architecture in the cat's visual cortex". In: *The Journal of Physiology* 160.

Huffman, Russell F. and Odell W Henson (1990). "The descending auditory pathway and acousticomotor systems: connections with the inferior colliculus". In: *Brain Research Reviews* 15, pp. 295–323.

Hurley, Laura M. (2018). "Neuromodulatory Feedback to the Inferior Colliculus". In: *The Oxford Handbook of the Auditory Brainstem*.

James, Gareth et al. (2021). "An Introduction to Statistical Learning". In: *Springer Texts in Statistics*.

Kawai, Risa et al. (2015). "Motor Cortex Is Required for Learning but Not for Executing a Motor Skill". In: *Neuron* 86, pp. 800–812.

Kuwabara, Nobuyuki and John M. Zook (2000). "Geniculo-collicular descending projections in the gerbil". In: *Brain Research* 878, pp. 79–87.

Kwon, Sung Eun et al. (2016). "Sensory and decision-related activity propagate in a cortical feedback loop during touch perception". In: *Nature neuroscience* 19, pp. 1243–1249.

Lee, Charles C and Jeffery A. Winer (2008). "Connections of cat auditory cortex: I. Thalamocortical system". In: *Journal of Comparative Neurology* 507.

Lee, Sangkyun et al. (2017). "Visually Driven Neuropil Activity and Information Encoding in Mouse Primary Visual Cortex". In: *Frontiers in Neural Circuits* 11.

Lee, Seung-Hee and Yang Dan (2012). "Neuromodulation of Brain States". In: *Neuron* 76, pp. 209–222.

Lesicko, Alexandria et al. (2016). "Connectional Modularity of Top-Down and Bottom-Up Multimodal Inputs to the Lateral Cortex of the Mouse Inferior Colliculus". In: *The Journal of Neuroscience* 36, pp. 11037–11050.

Lesicko, Alexandria M.H. and Maria Neimark Geffen (2022). "Diverse functions of the auditory cortico-collicular pathway". In: *Hearing research*, p. 108488.

Lesicko, Alexandria M.H. et al. (2022). "Corticofugal regulation of predictive coding". In: *eLife* 11.

Li, Jingcheng et al. (2017). "Primary Auditory Cortex is Required for Anticipatory Motor Response". In: *Cerebral Cortex* 27, pp. 3254–3271.

Llano, Daniel Adolfo and S. Murray Sherman (2008). "Evidence for nonreciprocal organization of the mouse auditory thalamocortical-corticothalamic projection systems". In: *Journal of Comparative Neurology* 507.

Lohse, Michael et al. (2020). "Neural circuits underlying auditory contrast gain control and their perceptual implications". In: *Nature Communications* 11.

Lohse, Michael et al. (2021). "Subcortical circuits mediate communication between primary sensory cortical areas in mice". In: *Nature Communications* 12.

Ma, X and Nobuo Suga (2001a). "Corticofugal modulation of duration-tuned neurons in the midbrain auditory nucleus in bats". In: *Proceedings of the National Academy of Sciences of the United States of America* 98, pp. 14060–14065.

— (2001b). "Plasticity of bat's central auditory system evoked by focal electric stimulation of auditory and/or somatosensory cortices." In: *Journal of neurophysiology* 85 3, pp. 1078–87.

McGinley, Matthew J., Stephen V. David, and David A. McCormick (2015). "Cortical Membrane Potential Signature of Optimal States for Sensory Signal Detection". In: *Neuron* 87, pp. 179–192.

Metzger, Ryan R. et al. (2006). "Effects of Reward and Behavioral Context on Neural Activity in the Primate Inferior Colliculus". In: *The Journal of Neuroscience* 26, pp. 7468–7476.

Mulders, Wilhelmina H A M and Donald Robertson (2000). "Evidence for direct cortical innervation of medial olivocochlear neurones in rats". In: *Hearing Research* 144, pp. 65–72.

Nakamoto, Kyle T., Simon J. Jones, and Alan R. Palmer (2008). "Descending projections from auditory cortex modulate sensitivity in the midbrain to cues for spatial position." In: *Journal of neurophysiology* 99 5, pp. 2347–56.

Namboodiri, Vijay Mohan K et al. (2019). "Single-cell activity tracking reveals that orbitofrontal neurons acquire and maintain a long-term memory to guide behavioral adaptation". In: *Nature neuroscience* 22, pp. 1110–1121.

Oberle, Hannah M et al. (2022). "Synaptic mechanisms of top-down control in the non-lemniscal inferior colliculus". In: *eLife* 10.

Oliver, Douglas L (2005). "Neuronal Organization in the Inferior Colliculus". In: *The Inferior Colliculus*, pp. 69–114.

Olthof, Bas M J, Adrian Rees, and Sarah E Gartside (2019). "Multiple Nonauditory Cortical Regions Innervate the Auditory Midbrain". In: *The Journal of Neuroscience* 39, pp. 8916–8928.

Pachitariu, Marius et al. (2017). "Suite2p: beyond 10,000 neurons with standard two-photon microscopy". In: *bioRxiv*.

Patel, Mili B. et al. (2017). "Anatomical characterization of subcortical descending projections to the inferior colliculus in mouse". In: *Journal of Comparative Neurology* 525.

Peron, Simon P. et al. (May 6, 2015). "A Cellular Resolution Map of Barrel Cortex Activity during Tactile Behavior". In: *Neuron* 86.3, pp. 783–799.

Pologruto, Thomas A, Bernardo L. Sabatini, and Karel Svoboda (2003). "ScanImage: Flexible software for operating laser scanning microscopes". In: *BioMedical Engineering OnLine* 2, pp. 13–13.

Price, Caitlin N. and Gavin M. Bidelman (2021). "Attention reinforces human corticofugal system to aid speech perception in noise". In: *NeuroImage* 235, pp. 118014–118014.

Reale, Richard A. and Thomas J. Imig (1983). "Auditory cortical field projections to the basal ganglia of the cat". In: *Neuroscience* 8, pp. 67–86.

Romanski, Lizabeth M. and Joseph E LeDoux (1993). "Information cascade from primary auditory cortex to the amygdala: corticocortical and corticoamygdaloid projections of temporal cortex in the rat." In: *Cerebral cortex* 3 6, pp. 515–32.

Rowland, James M. et al. (2021). "Perception and propagation of activity through the cortical hierarchy is determined by neural variability". In: *bioRxiv*.

Ryan, Allen F. and J. Miller (1977). "Effects of behavioral performance on single-unit firing patterns in inferior colliculus of the rhesus monkey." In: *Journal of neurophysiology* 40 4, pp. 943–56.

Ryan, Allen F. et al. (1984). "Effects of reaction time performance on single-unit activity in the central auditory pathway of the rhesus macaque". In: *The Journal of neuroscience : the official journal of the Society for Neuroscience*.

Saldaña, Enrique, M Feliciano, and Enrico Mugnaini (1996). "Distribution of descending projections from primary auditory neocortex to inferior colliculus mimics the topography of intracollicular projections". In: *Journal of Comparative Neurology* 371.

Schnupp, Jan W. H., Israel Nelken, and Andrew J. King (2011). *Auditory Neuroscience: Making Sense of Sound*.

Schofield, Brett R. (2010). "Structural organization of the descending auditory pathway". In: *The Oxford Handbook of Auditory Science: The Auditory Brain*.

Sekaran, Nathiya Vaithiyalingam Chandra et al. (2021). "Patterns of Unilateral and Bilateral Projections From Layers 5 and 6 of the Auditory Cortex to the Inferior Colliculus in Mouse". In: *Frontiers in Systems Neuroscience* 15.

Senatorov, Vladimir V. and B. Hu (2002). "Extracortical descending projections to the rat inferior colliculus". In: *Neuroscience* 115, pp. 243–250.

Slater, Bernard J., Adam M. Willis, and Daniel Adolfo Llano (2013). "Evidence for layer-specific differences in auditory corticocollicular neurons". In: *Neuroscience* 229, pp. 144–154.

Slater, Bernard J. et al. (2019). "Thalamocortical and Intracortical Inputs Differentiate Layer-Specific Mouse Auditory Corticocollicular Neurons". In: *The Journal of Neuroscience* 39, pp. 256–270.

Smith, Philip H et al. (2012). "Thalamocortical projections to rat auditory cortex from the ventral and dorsal divisions of the medial geniculate nucleus". In: *Journal of Comparative Neurology* 520.

Souffi, Samira et al. (2021). "When and How Does the Auditory Cortex Influence Subcortical Auditory Structures? New Insights About the Roles of Descending Cortical Projections". In: *Frontiers in Neuroscience* 15.

Stanislaw, Harold and N Todorov (1999). "Calculation of signal detection theory measures". In: *Behavior Research Methods, Instruments, & Computers* 31, pp. 137–149.

Stebbings, Kevin A, Alexandria M H Lesicko, and Daniel Adolfo Llano (2014). "The auditory corticocollicular system: Molecular and circuit-level considerations". In: *Hearing Research* 314, pp. 51–59.

Stiebler, I. and Günter Ehret (1985). "Inferior colliculus of the house mouse. I. A quantitative study of tonotopic organization, frequency representation, and tone-threshold distribution". In: *Journal of Comparative Neurology* 238.

Stringer, Carsen and Marius Pachitariu (2019). "Computational processing of neural recordings from calcium imaging data". In: *Current Opinion in Neurobiology* 55, pp. 22–31.

Suga, Nobuo et al. (2002). "Plasticity and Corticofugal Modulation for Hearing in Adult Animals". In: *Neuron* 36, pp. 9–18.

Talwar, Sanjiv K., Paweł Musiał, and George L. Gerstein (2001). "Role of mammalian auditory cortex in the perception of elementary sound properties." In: *Journal of neurophysiology* 85 6, pp. 2350–8.

Vasquez-Lopez, Sebastian A. et al. (2017). "Thalamic input to auditory cortex is locally heterogeneous but globally tonotopic". In: *eLife* 6.

Wang, Xinjun et al. (2013). "Distribution of CaMKIIα expression in the brain in vivo, studied by CaMKIIα-GFP mice". In: *Brain Research* 1518, pp. 9–25.

Weedman, Diana L. and David K Ryugo (1996). "Pyramidal cells in primary auditory cortex project to cochlear nucleus in rat". In: *Brain Research* 706, pp. 97–102.

Williamson, Ross S. and Daniel B. Polley (2019). "Parallel pathways for sound processing and functional connectivity among layer 5 and 6 auditory corticofugal neurons". In: *eLife* 8.

Winer, Jeffery A. (2005). "Decoding the auditory corticofugal systems". In: *Hearing Research* 207, pp. 1–9.

Winer, Jeffery A. and Jorge J. Prieto (2001). "Layer V in cat primary auditory cortex (AI): Cellular architecture and identification of projection neurons". In: *Journal of Comparative Neurology* 434.

Winer, Jeffery A. et al. (1998). "Auditory cortical projections to the cat inferior colliculus". In: *Journal of Comparative Neurology* 400.

Winer, Jeffery A. et al. (2002). "Descending projections to the inferior colliculus from the posterior thalamus and the auditory cortex in rat, cat, and monkey". In: *Hearing Research* 168, pp. 181–195.

Xiong, Xiaorui R et al. (2015). "Auditory cortex controls sound-driven innate defense behaviour through corticofugal projections to inferior colliculus". In: *Nature Communications* 6.

Yan, Jun and Günter Ehret (2002). "Corticofugal modulation of midbrain sound processing in the house mouse". In: *European Journal of Neuroscience* 16.

Yan, Jun, Yunfeng Zhang, and Günter Ehret (2005). "Corticofugal shaping of frequency tuning curves in the central nucleus of the inferior colliculus of mice." In: *Journal of neurophysiology* 93 1, pp. 71–83.

Yan, Wei and Nobuo Suga (1998). "Corticofugal modulation of the midbrain frequency map in the bat auditory system". In: *Nature Neuroscience* 1, pp. 54–58.

Yang, Yoonsun, Joonyeol Lee, and Gunsoo Kim (2020). "Integration of locomotion and auditory signals in the mouse inferior colliculus". In: *eLife* 9.

Yatsenko, Dimitri, Edgar Y. Walker, and Andreas Savas Tolias (2018). "DataJoint: A Simpler Relational Data Model". In: *ArXiv* abs/1807.11104.

Yudintsev, Georgiy et al. (2021). "Evidence for layer-specific connectional heterogeneity in the mouse auditory corticocollicular system." In: *The Journal of neuroscience : the official journal of the Society for Neuroscience*.

Zhang, Y. and Nobuo Suga (2000). "Modulation of responses and frequency tuning of thalamic and collicular neurons by cortical activation in mustached bats." In: *Journal of neurophysiology* 84 1, pp. 325–33.

Zingg, Brian et al. (2017). "AAV-Mediated Anterograde Transsynaptic Tagging: Mapping Corticocollicular Input-Defined Neural Pathways for Defense Behaviors". In: *Neuron* 93, pp. 33–47.